VIBRATING KELVIN PROBE MEASUREMENTS OF A SILICON SURFACE WITH THE UNDERSIDE EXPOSED TO LIGHT

A Thesis
Presented to
The Academic Faculty

by

Megan Dukic

In Partial Fulfillment
of the Requirements for the Degree
Master of Science in Mechanical Engineering

Georgia Institute of Technology
December 2007

VIBRATING KELVIN PROBE MEASUREMENTS OF A SILICON SURFACE WITH THE UNDERSIDE EXPOSED TO LIGHT

Approved by:

Dr. Danyluk, Advisor
School of Mechanical Engineering
Georgia Institute of Technology

Dr. Hesketh
School of Mechanical Engineering
Georgia Institute of Technology

Dr. Melkote
School of Mechanical Engineering
Georgia Institute of Technology

Date Approved: August 24, 2007

ACKNOWLEDGEMENTS

I would like to thank my academic advisor, Dr. Steven Danyluk, for giving me the opportunity to engage in research at Georgia Tech. I would also like to thank Dr. Francis Mess for providing advice in not only academia, but in many other important areas of life. Without the two of them I could not have completed this thesis. Many thanks to Sergey, Fang, Vicky, Andrey and Travis for listening to repeated presentations on Friday afternoons. Their questions and curiosities have allowed my research to move in directions I wouldn't have considered otherwise. A special thanks to Dr. Anatoly Zharin for continuously providing a means of measurement, even when it was returned in pieces.

I would like to thank my family for always listening when I needed them the most; even if it was at an inconvenient time. I would also like to thank Ted Dukic for pushing me to pursue research just for the sake of learning.

I would like to especially thank Alex for continued support during a strange time in an unfamiliar city. Without his patience and generosity I would not have taken this direction in life.

TABLE OF CONTENTS

LIST OF TABLES

LIST OF FIGURES

LIST OF SYMBOLS

%A	Percent of absorbed light
A	Surface area of Kelvin probe tip
b	Proportionality constant for altered Helmholtz equation
C	Capacitance of parallel plate capacitor
c	Speed of light in a vacuum
C_{Air}	Capacitance of air
C_{eq}	Equivalent Capacitance
C_{ox}	Capacitance of silicon dioxide
d	Distance between Kelvin probe tip and a sample
d_0	Average distance between Kelvin probe tip and sample
d_1	Amplitude of vibration of Kelvin probe tip
d_{Air}	Average “thickness” of air
D_n	Diffusion constant of excess electrons
d_{ox}	Thickness of silicon dioxide
e	Unit charge of an electron
E_{FM}	Fermi level of metal
E_{FSi}	Bulk Fermi level of silicon
E_{ph}	Energy of a photon
F_N	Quasi-Fermi level of excess electrons
F_P	Quasi-Fermi level of excess holes
G_L	Number of electron-hole pairs created
h	Planck’s Constant

i	Current into Kelvin probe tip
I	Intensity of light in silicon wafer
I_0	Intensity of light just inside surface of silicon wafer
k	Boltzman constant
L_n	Diffusion length of excess electrons
n	Number of electrons
n_i	Number of intrinsic electrons
N_{ph}	Photon flux
p	Number of holes
p_{Acc}	Density of holes in accumulation region
p_i	Number of intrinsic holes
Q	Charge on a plate of parallel plate capacitor
Q_{ex}	Charge density of excited silicon wafer
Q_m	Charge density on metal surface
Q_s	Charge density in silicon wafer's accumulation layer
Q_{un}	Charge density of unexcited silicon wafer
$Q_{\Delta n}$	Charge density of excess electrons at front surface of silicon wafer
R	Reflectance of incident light
s_{FRONT}	Recombination velocity at front surface of silicon wafer
s_{REAR}	Recombination velocity at back surface of silicon wafer
T	Temperature
t	Time
V	Voltage of parallel plate capacitor
V_A	Voltage applied to metal
V_{cpd}	Voltage difference between Kelvin probe tip and sample

V_{ex}	Excited voltage output
V_p	Output Voltage of probe
$V_{p,un}$	Output Voltage of probe without illumination
$V_{p,ex}$	Output Voltage of probe with illumination
V_s	Compensating voltage source
V_{un}	Unexcited voltage output
x	Depth into silicon wafer
α	Absorption coefficient
Δn	Change in number of electrons due to light
Δp	Change in number of holes due to light
ΔV	Voltage difference between excited and unexcited silicon wafer
$\Delta\varphi_s$	Change in surface potential between excited and unexcited silicon wafer
ε_0	Permittivity of free space
ε_{Air}	Dielectric constant of air
ε_{ox}	Dielectric constant of silicon dioxide
ε_S	Dielectric constant of silicon
θ	Fractional surface coverage of adsorbate species
λ	wavelength of light
ρ	Charge density of silicon wafer
τ_n	Average electron lifetime
τ_p	Average hole lifetime
Φ_{M1}	Work function of Metal 1
Φ_{M2}	Work function of Metal 2
φ_s	Surface potential of silicon wafer
ω	Frequency of vibration of Kelvin probe tip

SUMMARY

This thesis addresses the use of a vibrating Kelvin probe to monitor the change in the front surface potential of a silicon wafer while the rear surface is illuminated with monochromatic, visible light. Two tests were run to verify the change in surface potential. One test increased the intensity of the light and the other increased the wavelength while recording the front surface potential.

The change in the surface potential for a range of intensities of incident light was recorded and analyzed. The results show that the change in surface potential increased with increasing intensity. For each wafer, the smallest change in surface potential occurred at the lowest intensity, 3.77 mW. In the same respect, the largest change in surface potential occurred at the highest intensity, 17.8 mW. For all wafers, the change in surface potential ranged from approximately 8 mV at 3.77 mW to approximately 80 mV at 17.8 mW.

The change in the surface potential for a range of wavelengths of incident light was also recorded and analyzed. The results showed that the change in surface potential formed a skewed bell curve with increasing wavelength of incident light. For each wafer, the largest change in surface potential occurred at mid-range wavelengths, between 600 nm and 700 nm. The smallest change in surface potential occurred at 450 nm, the shortest wavelength, and 800 nm, the longest wavelength. For all wafers, the change in surface potential ranged from approximately 8 mV at 800 nm to approximately 165 mV at 700 nm.

A model based on excess electron diffusion within the silicon wafer was used to predict material properties. After curve fitting the model with experimental results, an excess electron lifetime of $\tau_N = 17$ μs and surface recombination rates of $s_{FRONT} = s_{REAR} =$ 18,000cm/s were predicted. These values suggest poor silicon wafer quality relative to commercial silicon devices.

Regardless of the quality, the results show that the front surface potential of a silicon wafer is affected by incident light on the rear surface. The quantitative effect of the light is dependent on the properties of the light and the material properties of the silicon wafer.

CHAPTER 1

INTRODUCTION

This thesis addresses the use of a vibrating Kelvin probe to monitor the potential on the front surface of a silicon wafer while shining visible light on the rear surface. A change in the front surface potential between an excited state, in which incident light was present, and an unexcited state, whereby no light was present, was found to be dependent on both the wavelength and intensity of the light.

The voltage output of the Kelvin probe sensor can be attributed to physical mechanisms occurring inside the silicon wafer. First, is the flow of electrons from the silicon wafer into the Kelvin probe tip until a uniform Fermi energy is achieved. This creates a slight negative charge on the probe tip and a positively charged accumulation region near the front surface of the silicon wafer. As the probe tip begins to vibrate, electrons mobilize and cyclically alter the electric field between the probe tip and the front surface of the wafer at the probe tip's vibration frequency. Excess electron-hole pairs are created near the rear surface of the silicon wafer when exposed to light. The excess amount of electrons at the rear surface will diffuse throughout the wafer until a steady-state distribution is achieved. Many of the electrons will diffuse into the accumulation region at the front surface of the silicon and thus, alter the output voltage of the Kelvin probe.

Proof of this concept was achieved by monitoring the front surface potential of the wafer while light was pulsed on the rear surface at 20 second intervals. A vibrating

Kelvin probe sensor equipped with a voltage feedback-biasing probe tip was used to monitor the potential difference between the probe tip and the silicon wafer. When the wafer was exposed to light, the output voltage decreased from an unexcited value to a saturated excited value. When the light was removed, the output voltage increased and returned to the unexcited value. Hence, the transition period between the successive excited voltage values matched the period of the on/off light cycle. Once this was observed, a number of experiments were performed in which the light's wavelength and intensity were systematically increased. The repeatable outcomes of the experiments verified that the front surface potential of the silicon wafer was dependent on both the wavelength and intensity of the incident light. A predictive model was created to determine properties of the silicon wafer, given the geometry of the measuring system and the wavelength and intensity of the incident light.

This system can potentially be used in industry as either an actuator or a sensor. A desired surface potential can be created on a silicon wafer by altering only the intensity or wavelength of light shown on the rear surface. The controlled potential can be used to drive additional circuitry. Since this system is made of silicon, the package could be downsized and easily integrated. On the other hand, this system can be altered to create a novel, non-vibrating Kelvin probe sensor. Without vibration, the method of signal generation is the changing surface potential of the silicon wafer due to pulsed incident light. The sensor is sensitive to any process that alters the work function of the surface of the silicon wafer, such as adsorption, surface defects, and stress. Age testing of motor oil with a similar optically stimulated sensor was successfully performed by Dr. Francis Mess in the Electronic Materials Lab located at Georgia Tech. The contactless nature of

the probe coupled with rear surface incident light creates a sensor in which the measurand, the front surface of the wafer, is unaltered.

CHAPTER 2

BACKGROUND

Contact Potential Difference

The contact potential difference is defined as the potential developed between the surfaces of two dissimilar metals brought into close proximity while electrically connected. The potential is a result of the exchange of electrons, via the electrical connection, from the metal with the higher Fermi level to the other until a uniform Fermi level is reached. This process is shown in Figure 2.1.

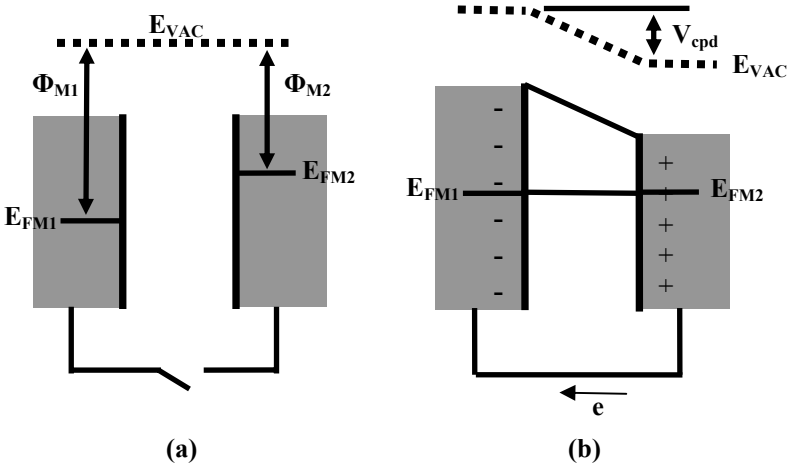

Figure 2.1 Energy diagram of the Fermi-level equilibrium model when two metals are (a) disconnected and (b) connected.

The value of the contact potential difference resulting from the exchange of electrons can be described in terms of each metal's work function, as shown in equation

2.1. The work function of a metal is the amount of energy an electron needs to be completely removed from the bulk to a vacuum energy level just outside the surface.

$$V_{cpd} = \frac{\Phi_{M1} - \Phi_{M2}}{|e|} \tag{2.1}$$

In the above, Φ_{M1} is the work function of metal 1, Φ_{M2} is the work function of metal 2, and e is the unit charge of an electron. If the metal plates are parallel, the two plates will behave like a parallel plate capacitor, in which the charge on each plate is proportional to the potential. The proportionality constant is the capacitance. The contact potential difference can be described by:

$$V_{cpd} = \frac{Q}{C} \tag{2.2}$$

where Q is the charge on each metal plate and C is the capacitance of the dielectric material separating the plates. The charge on each plate is a result of the electron transfer between the metals. If air acts as the dielectric between the two plates, the capacitance used in equation 2.2 can be determined from:

$$C = \frac{\varepsilon_o \varepsilon_{Air} A}{d} \tag{2.3}$$

where ε_o is the permittivity of free space, ε_{Air} is the dielectric constant of air, A is the area of each metal plate, and d is the distance between plates. The exchange of the electrons is time dependent. Thus, a current exists in the wire connecting the two plates.

$$i = \frac{\partial Q}{\partial t} = V_{cpd}\frac{dC}{dt} + C\frac{dV_{cpd}}{dt} \tag{2.4}$$

By measuring the current in the connecting wire, a sensor can be created that is sensitive to a change in capacitance or potential. Different devices have been designed based on equation 2.4 [1]. The most relevant is the Kelvin probe.

The Vibrating Kelvin Probe

In this thesis, the vibrating Kelvin probe was used to take measurements. The Kelvin probe is named after Lord Kelvin. In 1898, he published an experiment based on the transport of "electricity" between two dissimilar metals [2]. He described the movement caused by Coulomb repulsion within a gold leaf electroscope when he brought zinc and copper plates into close proximity while the plates were electrically connected. In 1932, Zisman suggested an improved method for quantifying the potential difference between two metal plates[3]. He vibrated one of the metal plates relative to the other in order to take continuous measurements of the potential difference.

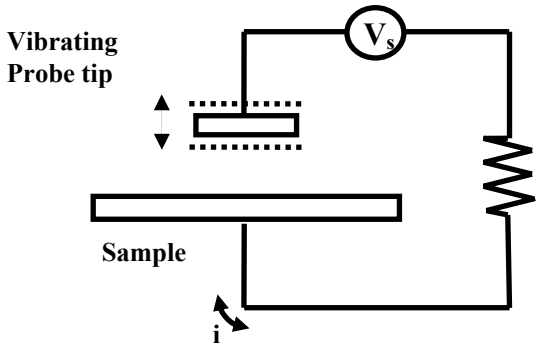

Figure 2.2 Diagram of the vibrating Kelvin probe.

A vibrating Kelvin probe consists of vibrating a metal probe tip with a known Fermi level above a metallic sample with unknown properties while the metals are electrically connected. A diagram of a typical vibrating Kelvin probe is shown in Figure 2.2. As the probe tip vibrates, a current induced by the vibration moves between the plates via the electronic connection. By assuming constant experimental conditions, the potential difference remains constant, i.e. $\frac{dV}{dt} = 0$.

Hence, equation 2.4 can be simplified.

$$i = V\frac{dC}{dt} \tag{2.5}$$

The varying capacitance is a result of the vibration of the reference metal. The vibration is controlled. Hence, the distance between the metal plates can be described as a sinusoid with known properties

$$d = d_0 + d_1 \sin \omega t \tag{2.6}$$

where d_0 is the average distance between plates, d_1 is the amplitude of vibration and ω is the frequency of vibration. After differentiation, the current flowing between the metals is shown in equation 2.7.

$$i = -V \frac{\varepsilon_0 \varepsilon_{Air} A d_1 \omega \cos \omega t}{(d_0 + d_1 \sin \omega t)^2} \tag{2.7}$$

To find the contact potential (V) in a lab setting, an adjustable voltage source can be added to the circuit, as shown in Figure 2.2.

$$i = (V_s - V) \frac{\varepsilon_0 \varepsilon_{Air} A d_1 \omega \cos \omega t}{(d_0 + d_1 \sin \omega t)^2} \tag{2.8}$$

In the above, V_s is the voltage source added to the circuit to provide a compensating voltage to the probe tip. The voltage source is adjusted until there is no current flowing between the tip and the sample, i.e. i(t)=0. When this occurs, the voltage provided by the voltage source is equal to the potential between the reference plate and the sample [3]. This is verified by equation 2.8 and it is commonly referred to as the null method.

The Kelvin probe is used to detect a material's surface condition. It is known that the work function of a metal can be altered by certain surface conditions such as stress, corrosion and adsorption. A correlation between the work function and the surface condition can be found by simultaneously monitoring the surface potential with a Kelvin

probe and the surface condition with an additional measuring device. This technique has been utilized to determine the stress in a flexed beam [4], the electrochemical state of a metal's surface during corrosion [5], and the bonding energy of an adsorbate species [6]. The Kelvin probe tip can also be scanned across a sample surface. The scanning-vibrating Kelvin probe has been used to successfully detect localized potential differences induced by adsorption [7], surface wear during sliding [8, 9], and oxidation [9].

Because of the Kelvin probe's sensitivity to ambient conditions, care must be taken in the selection of the probe tip material and testing environment. The material of the Kelvin probe tip should have a low reactivity and all experiments should be performed within a vacuum to control environmental conditions [10].

The Metal-Insulator-Semiconductor Capacitor (MIS-C)

When a metal plate and semiconductor wafer are brought into close proximity while electrically connected, a contact potential difference will develop between the two materials. As mentioned earlier, electrons will momentarily flow from one material into the other until a uniform Fermi level is reached. The metal-insulator-semiconductor capacitor (MIS-C) takes advantage of this phenomenon. A diagram of MIS-C is shown in Figure 2.3.

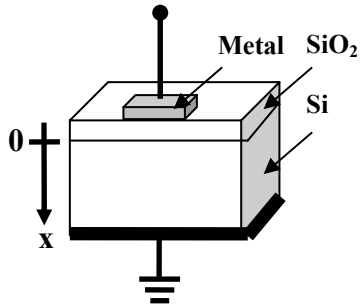

Figure 2.3 Model of a MIS-C device.

However, the contact potential difference resides in the dielectric material and in a small region just inside the semiconductor near the semiconductor-insulator interface. The energy band model for the MIS-C is shown in Figure 2.4.

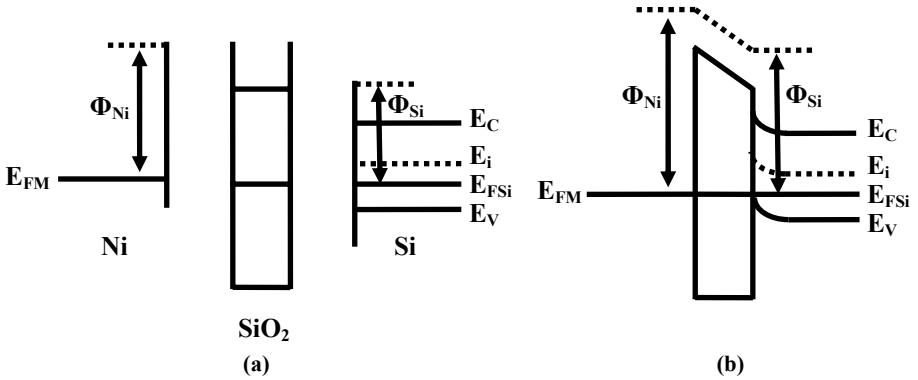

Figure 2.4 Energy diagram of the Fermi-level Equilibrium model for a MIS-C device when the materials are (a) separated and (b) connected. The metal is nickel, the insulator is silicon dioxide and the semiconductor is p-type silicon.

The MIS-C is a frequently used electronic device. The structure is well documented and fundamental equations describing MIS-C behavior are commonly verified in literature. All information presented in this section referenced material in textbooks written by Sze and Pierret [11, 12].

The measuring device used in all experiments can be modeled as a MIS-C. The metal was nickel, the insulator was both air and silicon dioxide (SiO_2), and the semiconductor was a p-type silicon wafer. For simplicity, those materials and their properties are used to describe the function of the MIS-C.

It is common practice to apply a voltage to the metal plate of the MIS-C. This will either raise or lower the equipotential Fermi level of the metal depending on the polarity of the applied voltage. This, in turn, will affect the electric field inside the insulator and near the surface of the semiconductor. When the exterior voltage is applied, the Fermi level equilibrium model does not apply. The separation of the Fermi levels will be equal to the applied voltage as shown in equation 2.9.

$$E_{FM} - E_{FS} = -eV_A \tag{2.9}$$

In the above, E_{FM} is the Fermi energy of the metal, E_{FS} is the Fermi level of the semiconductor and V_A is the applied voltage. The qualitative effect of the addition of a voltage to the metal of a MIS-C is shown in Figure 2.5.

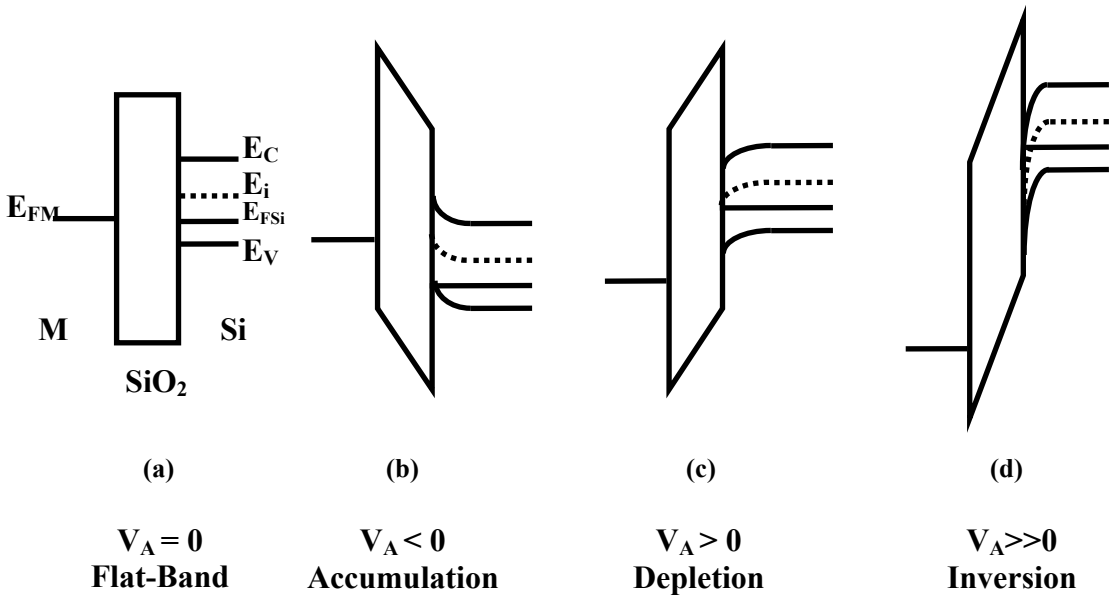

Figure 2.5 Energy diagram for a MIS-C device when a voltage is added to the metal for (a) Flat-band, (b) Accumulation, (c) Depletion, and (d) Inversion states in the semiconductor. For simplicity, the metal and the semiconductor share the same Fermi-level. The semiconductor is assumed to be p-type.

In three of the four scenarios in Figure 2.5, a voltage is applied to the metal, and the energy bands of all three materials are altered. Each of these cases has slightly different electronic properties. The cases are known as: flat-band, accumulation, depletion and inversion. The depletion case is the most common mode of operation in semiconductor devices. It occurs when a positive voltage is applied to the metal which causes a negatively charged region near the surface of the silicon. The negative charge is a result of the holes scattering towards the bulk of the silicon leaving behind only negatively charged ions in the silicon's lattice. The measurement device used in all experiments described in this thesis operates in a state of accumulation. In this state, a positive charge accumulates just inside the silicon surface due to the gathering of positively charged holes.

Thus, the electronic properties of a MIS-C are dependent on the movement of charged particles. By adding an exterior voltage to the system, the movement of charged particles is manipulated. The opposite phenomenon, the change in potential brought on by the movement of charged particles within the semiconductor, can occur and will be explained farther in the modeling section.

Photovoltaic Effect

When light impinges on a semiconductor, a portion of the light will be absorbed. The absorbed light will lose energy in the absorption proven by the creation of electron-hole pairs and heat in the form of phonons. The electron-hole pairs are mobile and will affect the electronic properties of the wafer. When the light is removed, the electron-hole pairs will recombine until the wafer's electronic properties return to their previous values. The creation of electron-hole pairs by illumination is a well documented phenomenon. All equations in this section were found in textbooks written by Sze and Pierret [11, 12].

The amount of incident light absorbed by a semiconductor wafer is dependent on the energy and wavelength of the photons hitting the wafer. Equation 2.10 describes the energy of a photon associated with monochromatic light.

$$E_{ph} = \frac{hc}{\lambda} \tag{2.10}$$

In the above, h is Planck's constant, c is the speed of light in a vacuum, and λ is the wavelength of the light. If the energy of each photon is greater than the band gap energy of the semiconductor, the light will be absorbed.

Not all of the photons are absorbed at the semiconductor's surface. Depending on the wavelength of a photon, it can travel well into the bulk of the wafer before it is absorbed. Hence, the penetration depth is also dependent on the wavelength. The average penetration depth is the inverse of the adsorption coefficient, α, which is a material property verified experimentally. A graphical representation of adsorption coefficient values for a silicon wafer for a range of wavelengths is shown in Figure 2.6. The adsorption coefficient was quantified only for the discrete wavelength values used in experimentation. Each wavelength is marked with an "X" in Figure 3.4.

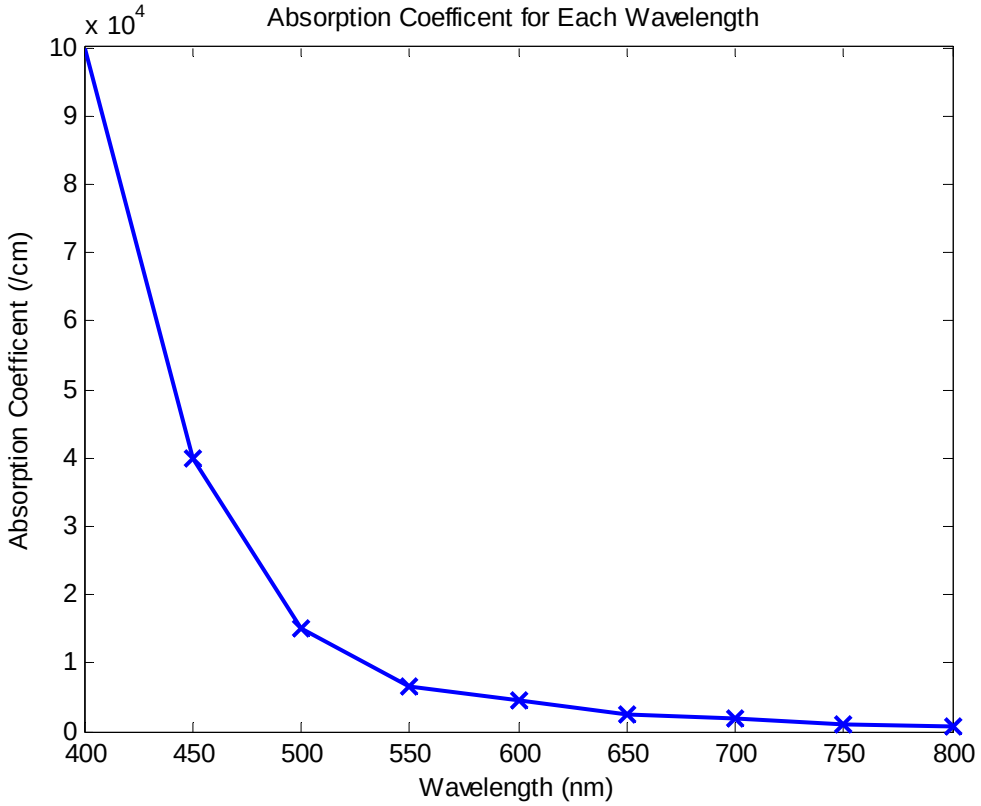

Figure 2.6 Adsorption Coefficient vs. wavelength of incident light for silicon [40]. Each marked value coincides with a wavelength relevant to experimentation.

The intensity of the light as it comes into contact with the wafer is given by:

$$I(x) = I_0 \bullet e^{(-\alpha x)} \tag{2.11}$$

where I is the intensity of light, I_0 is the intensity of light just inside the surface, α is the absorption coefficient, and x is the penetration depth into the silicon. The intensity decays as it is absorbed by the wafer. Each absorbed photon will create a single electron-hole pair. This one-to-one ratio gives rise to the electron-hole pair creation rate described by:

$$G_L(x) = (1-R)N_{ph}\alpha e^{(-\alpha x)} \tag{2.12}$$

where G_L is the number of electron-hole pairs created, R is the percent of light reflected, α is the absorption coefficient and N_{ph} is the photon flux. As with intensity, the creation of electron-hole pairs will decrease with increased penetration depth. Once the electron-hole pairs are created, the electron-hole pairs are free to move. Thus, the electron-hole pairs greatly affect the electronic properties of the wafer. The movement of charged particles and the affect on electronic properties will be explained in the modeling section.

As detailed earlier, a semiconductor exposed to light will no longer be in equilibrium. Thus the Fermi level cannot be represented on an energy band diagram. Instead, two quasi-Fermi levels are drawn, one for the number of electrons and the other for the number of holes. Equations 2.13a and 2.13b show the electron and hole quasi-Fermi levels.

$$F_n = E_i + kT \ln\left(\frac{n}{n_i}\right) \tag{2.13a}$$

$$F_P = E_i + kT \ln\left(\frac{p}{p_i}\right) \tag{2.13b}$$

In the above, E_i is the intrinsic Fermi level, k is the Boltzman constant, T is the temperature, p (n) is the number of holes (electrons), and p_i (n_i) is the number of intrinsic holes (electrons). The quasi-Fermi levels can be used to verify electronic properties within a wafer. The energy diagram of a semiconductor with quasi-Fermi levels is shown in Figure 2.7.

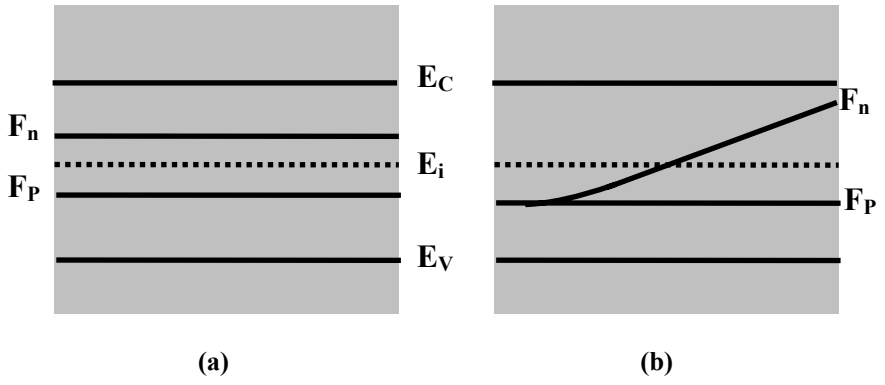

Figure 2.7 Energy diagram of a p-type Si wafer exposed to (a) constant illumination throughout the wafer and (b) right-side surface illumination. The Quasi-Fermi levels represent non-equilibrium operation.

While excess electron-hole pairs are created by exterior light, a number are also annihilated by recombination. During light absorption, the amount of electron-hole pairs created far outnumbers those that recombine. Therefore, excess carriers are present within the wafer. However, when the light is removed, the recombination process will dominate until all of the excess electron-hole pairs are destroyed and the semiconductor returns to equilibrium. The dominate recombination process in silicon is charge center recombination. This phenomenon is a result of allowed energy levels within the forbidden energy gap. This process is described by equation 2-14a and 2-14b for electrons and holes respectively.

$$\left.\frac{\partial p}{\partial t}\right|_R = -\frac{\Delta p}{\tau_p} \tag{2.14a}$$

$$\left.\frac{\partial n}{\partial t}\right|_R = -\frac{\Delta n}{\tau_n} \tag{2.14b}$$

In the above, Δp (Δn) is the change in the number of holes (electrons) from the bulk number of holes (electrons), and τ_p (τ_n) is the average hole (electron) lifetime.

The average lifetime for carriers in a semiconductor is dependent on conditions inside the semiconductor and usually ranges from 1 ms to 100 ns. For a doped semiconductor, the lifetime of a hole will differ from that of an electron, as seen in equations 2-14a and 2-14b. The lifetime can also vary within a wafer based on local lattice conditions. Hence, a measurement of the average carrier lifetime within a given wafer is needed if an accurate rate of recombination is desired.

The Kelvin Technique Applied to Semiconductor Samples

Vibrating Kelvin probes can also be used to detect surface conditions of a semiconductor sample. However, unlike a metal, the potential at the surface of the semiconductor may differ from the bulk [13]. Also, the conductance of a semiconductor can change readily. Because of this, the behavior of semiconductors is generally more complex than metals. The behavior of p-type silicon was explained in the previous section.

The vibrating Kelvin probe is used extensively in the semiconductor industry to quantify material properties. During semiconductor manufacturing, Kelvin probes are used to monitor impurity level [14], surface contamination [15], oxide thickness [16], and trapped surface charge [17-19]. All of the above will affect the electronic properties of a semiconductor and must be monitored during fabrication to ensure proper device operation.

As semiconductor devices become smaller in size, the properties of the device must be monitored at a smaller scale. Because of the advanced resolution of the scanning-vibrating Kelvin probe, it can be used to monitor surface defects [20] and grain boundaries [21] on a nanometer scale. Both of which can have an adverse effect on signal properties of a nano-scale device.

A semiconductor's electronic properties are altered when exposed to light due to the photovoltaic effect. The light causes excess charged carriers in the semiconductor. The effect of light on p-type silicon was described in the previous section. The properties associated with the excess charged particles, such as lifetime, can be determined by monitoring the surface potential of a semiconductor exposed to light [22]. The probe tip

is perforated so that light can pass though it and hit the top surface of the semiconductor wafer. The configuration is shown in Figure 2.8.

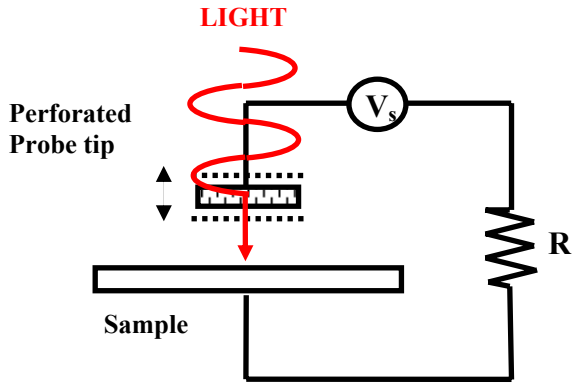

Figure 2.8 Diagram of a vibrating Kelvin probe monitoring the surface of a semiconductor wafer exposed to light.

Additional properties of excess charges particles, such as diffusion length, can be calculated by depositing a known charge on the surface of a semiconductor wafer and then exposing it to light while monitoring the surface with a vibrating Kelvin probe [23]. The configuration is also described by Figure 2.8.

The Optically Stimulated Contact Potential Difference Probe

A novel sensor has been created in the Electronic Materials Lab at Georgia Tech by combining the operation of the Kelvin probe with the photovoltaic effect of silicon. The device, called the optically stimulated contact potential difference sensor (osCPD sensor), was proven sensitive to the degradation of motor oil [24]. It consists of a non-vibrating Kelvin probe and an optically stimulated silicon wafer. A diagram of the osCPD is shown in Figure 2.9.

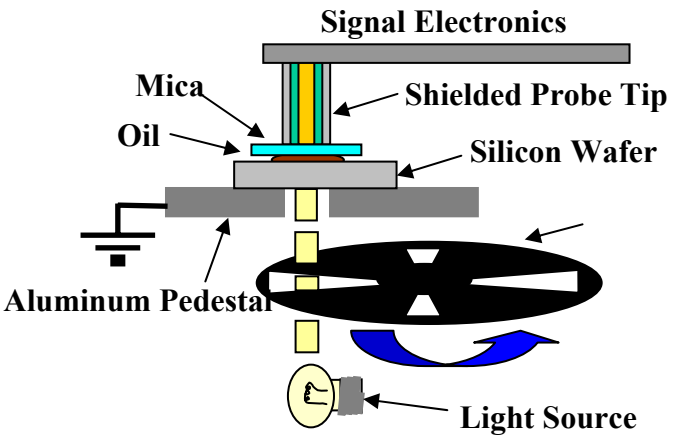

Figure 2.9 Diagram of the osCPD sensor.

The current detected in the probe tip is described by equation 2.3. The distance between the probe tip and silicon wafer is held constant, which results in a constant capacitance. Hence, the current is reduced to

$$i = C\frac{d\phi_s}{dt} \tag{2.15}$$

where φ_s is the surface potential of the silicon wafer. The surface potential is modulated by pulsed light on the rear surface of the silicon wafer, thus, providing a constantly varying current in the probe tip. The potential is dependent on the frequency of the pulses and properties of the light.

The measurand is a fluid placed on the silicon wafer. In theory, the fluid will influence the work function of the silicon by way of adsorbing to the surface. This will, in turn, affect the current measured by the probe tip.

Tests were performed on numerous samples of commercial grade motor oil. Chemical changes associated with degradation and contamination of the oil were detected with the osCPD sensor. The results of the experiments correlated well with results obtained from other forms of testing, such as optical spectroscopy [24].

CHAPTER 3

EXPERIMENTATION, MODELING, AND SIMULATION

The Experimental Apparatus

In the experiments presents in this thesis, a vibrating Kelvin probe was used to measure the contact potential difference between a nickel probe tip and a silicon wafer. During measurement, the rear surface of the silicon wafer was exposed to light as seen in Figure 3.1.

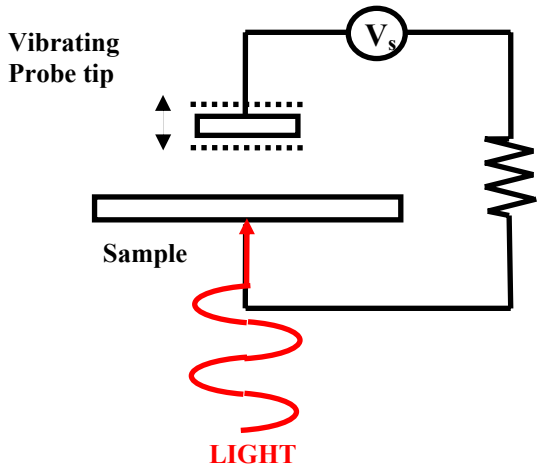

Figure 3.1 Diagram of the experimental setup.

The measuring system contained an aluminum fixture, a plastic enclosure, a vibrating Kelvin probe, a light source, and a PC-aided data acquisition system. A picture of the measuring system is shown in Figure 3.2.

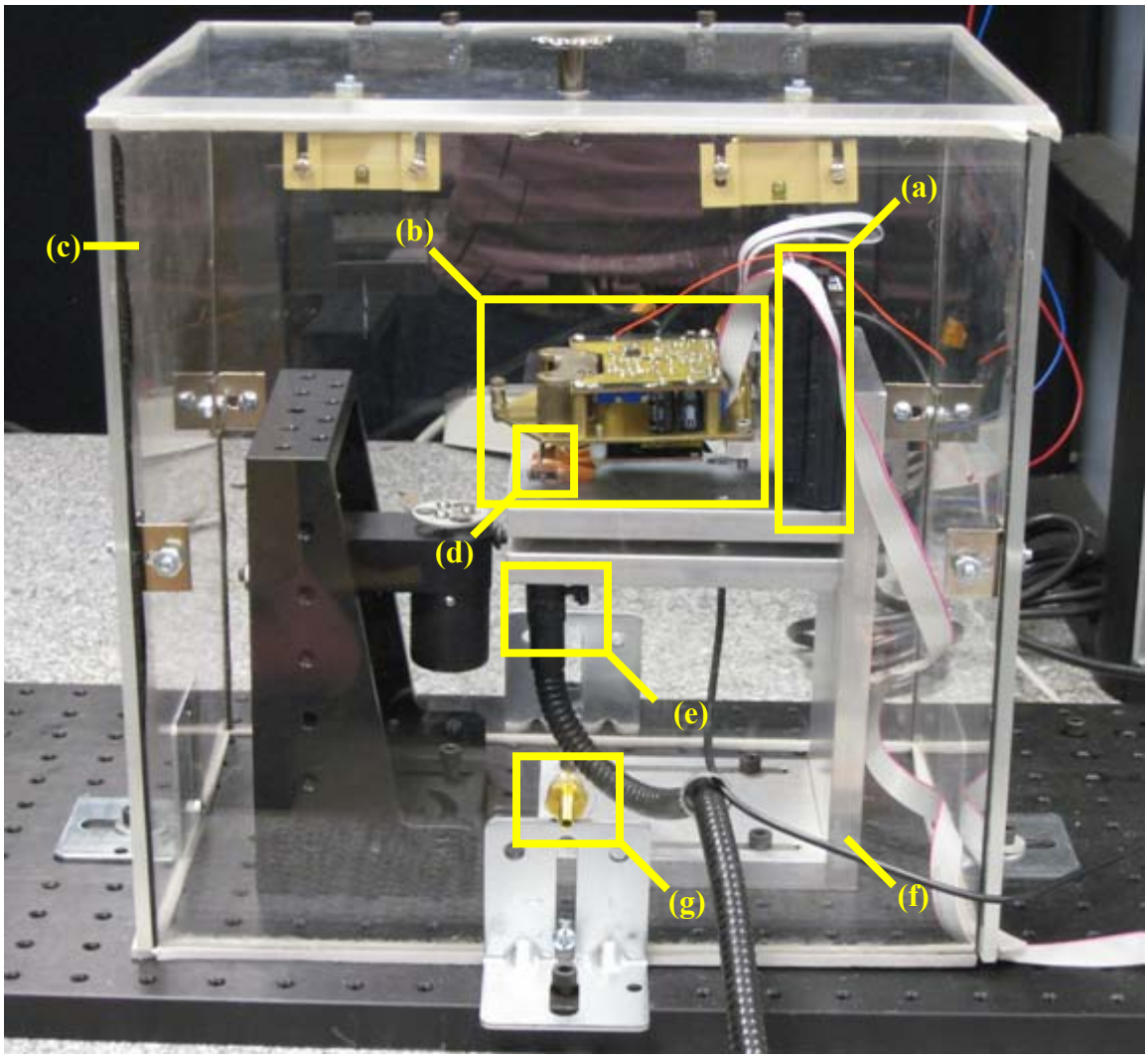

Figure 3.2 Picture of the measuring device. Components: (a) Micrometer Positioning Device (b) Vibrating Kelvin Probe (c) Isolation Box (d) Kelvin Probe Tip (e) Light Pipe (f) Aluminum Fixture (g) Nozzle

The aluminum fixture, shown in figure 3.3, was designed to align the probe tip, the silicon wafer and the light source.

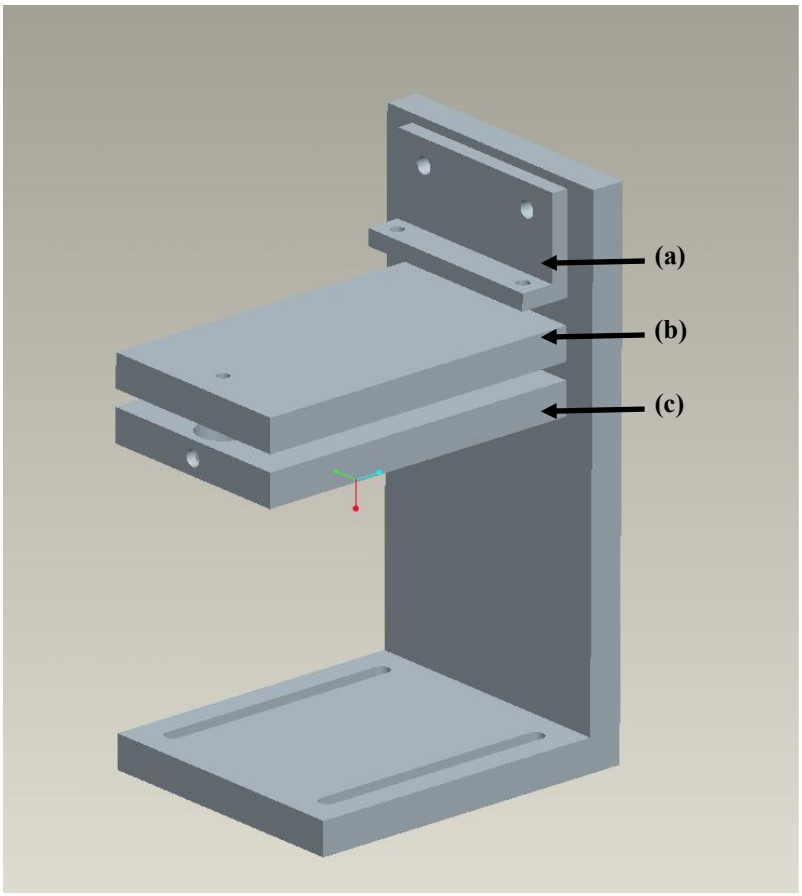

Figure 3.3 Drawing of the aluminum fixture used for alignment. (a) probe tip bracket (b) silicon wafer pedestal with light aperture (c) light pipe holder

It consists of a rectangular pedestal with a 1.0 cm diameter hole, over which a silicon wafer is placed. The hole is a light aperture. Positioning pins are located on two sides of the aperture to aid in centering the wafer above it. Copper tape surrounds the aperture to create an ohmic contact with the wafer. The copper is attached to a common ground, effectively grounding the back-side of the wafer. A bracket is attached to a micrometer positioning device used to hold the probe tip directly above the wafer, as shown in Figures 3.2 and 3.3. The distance between the probe tip and the wafer can be adjusted in 1 mm increments by lowering the probe tip with the positioning device. A second pedestal sits 0.5" below the first, as shown in Figure 3.3. It contains a 0.5" diameter hole

used to hold a light pipe and a single wavelength filter directly below the aperture. The light pipe, the aperture hole, and the probe tip need to be in alignment to ensure repeatable measurements. The aluminum fixture is attached to a heavy plate to reduce vibration.

The aluminum fixture is completely enclosed in a rectangular Plexiglas box, shown in Figures 3.2 and 3.4.

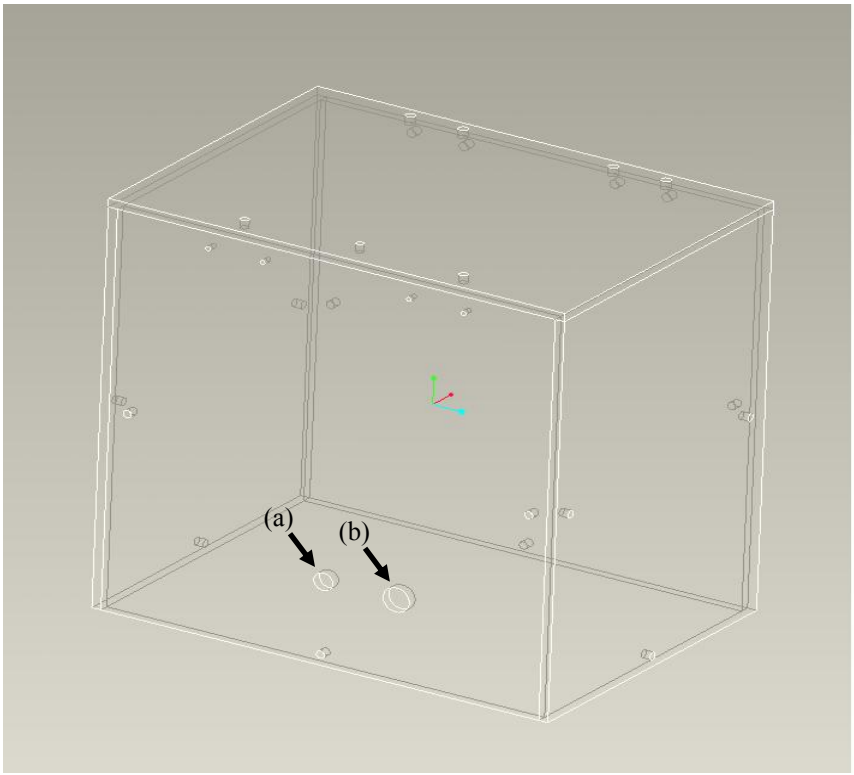

Figure 3.4 Drawing of the isolation box used to maintain a static testing environment. (a) nozzle placement (b) light pipe access

Access to the fixture is achieved by opening the hinged top. The box is sealed at all corners with foam tape. The light pipe and the data acquisition wires are threaded through a small hole on the front surface of the box to create a connection between the sensor and an exterior power and light source. A nozzle is also located on the front surface so that a 3/8" rubber hose can be attached to fill the box with a desired gas, as

shown in Figure 3.4. The purpose of the box is to maintain a uniform environment by minimizing fluctuations in ambient conditions. Ambient light is eliminated by covering the box.

Light from an exterior projector bulb is focused on the back of the silicon wafer by way of a light pipe. The intensity of the light can be adjusted as a percentage of the bulb's maximum intensity, 17.8 mW. The intensity was quantified by a visible light meter. A graph of power percentage vs. intensity is shown in Figure 3.4. The power was quantified only for the discrete intensity values used in experimentation. Each intensity is marked with an "X" in Figure 3.5.

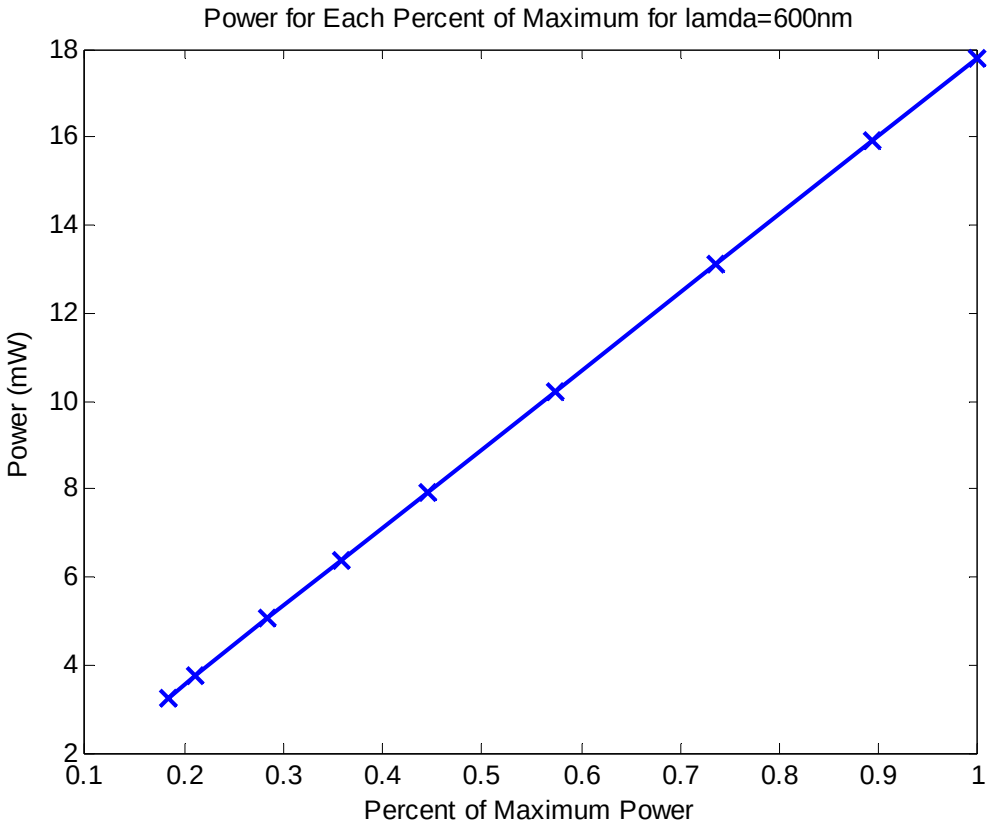

Figure 3.5 The power for each percentage setting of the light source. Each marked value coincides with an intensity relevant to experimentation.

The wavelength of the light is controlled by attaching a band-pass filter to the light pipe. The band-pass filters range from 400 nm - 800 nm in 50 nm increments. The maximum power for each wavelength was also quantified by a visible light meter. A graph of the maximum power vs. wavelength is shown in Figure 3.6. The maximum power is 17.8 mW and occurs at 600 nm. The power was quantified only for the discrete wavelength values used in experimentation. Each wavelength is marked with an "X" in Figure 3.4.

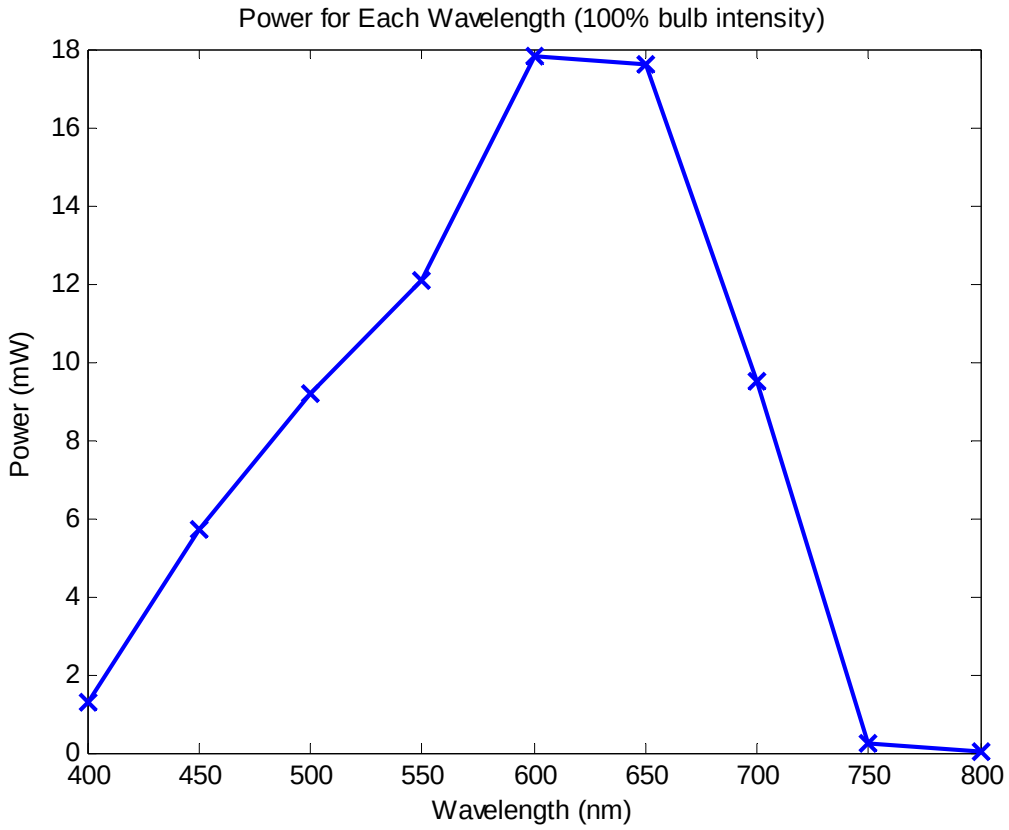

Figure 3.6 The maximum power for each wavelength of the light source. Each marked value coincides with a wavelength relevant to experimentation.

The vibrating Kelvin probe, shown in figure 3.7, was built by Dr. Anatoly Zharin.

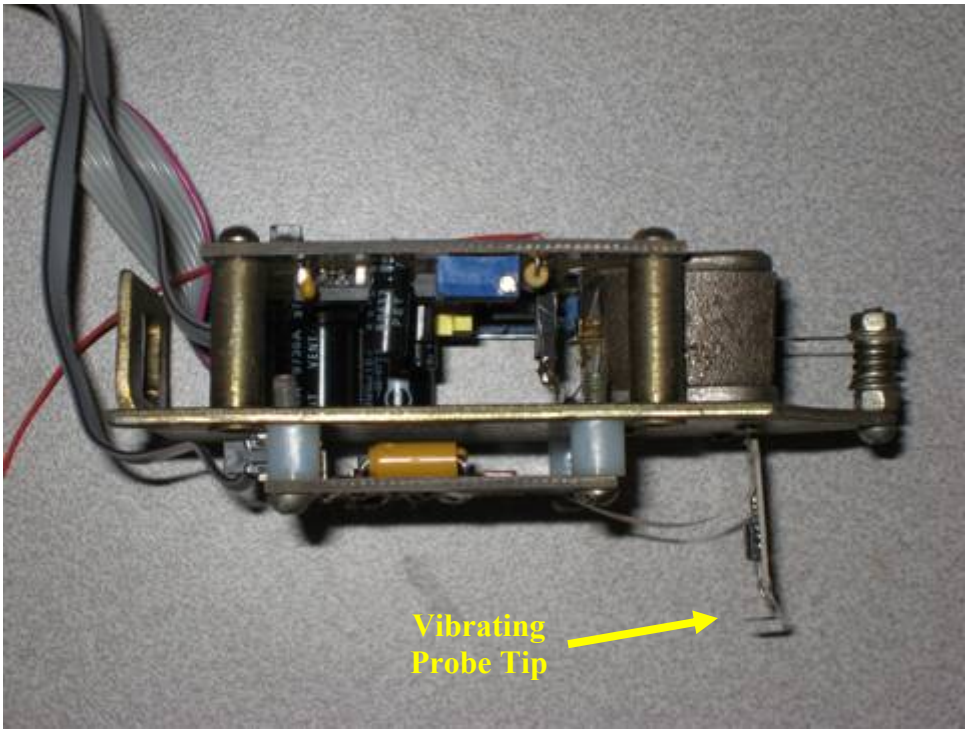

Figure 3.7 Picture of the Kelvin Probe.

It is driven by a ±12 V power source. The probe tip is made of nickel and has a surface area of 2 cm^2. A lock-in amplifier adjusted to the probe tip's vibration frequency and a voltage source are combined to provide the continuous feedback voltage needed to null the current in the tip[25].

A SCB-68 shielded interface box, a PCI-6052E data acquisition card and a Labview program are integrated to record all output measurements. The output signal from the probe is directly fed into the interface box, where it is compared to a common ground. The Labview program is designed to read a DC voltage in a series of digitized increments. All of the parameters are adjustable according to the user's needs. The

program's user interface and block diagram can be found in Appendix B. All voltage values are saved in a specified text document, which is labeled according to the date taken, wafer tested, and incident light parameters. The files are later analyzed with Matlab software.

The Experimental Procedure

Measurements were made using a 6" silicon wafer diced into 10 mm x 10 mm squares. Key properties of the wafer are listed in Table 3.1.

Table 3.1 Properties of the silicon wafer

Growth Method	Cz
Crystal Orientation	<111>
Dopant	Boron
Surface Finish	Polished
Diameter	125 mm
Dice size	10 mm x 10 mm
Thickness	650 μm
Resistivity	20 Ωcm

After dicing, each wafer is rinsed in a methanol bath and then with DI water. Each wafer is cleaned no more than three hours prior to experimentation.

The cleaned wafer is placed on the pedestal above the light aperture and centered via alignment pins. The probe tip is lowered so that it is approximately 1 mm above the silicon wafer's surface. The desired band-pass wavelength filter is placed on the light pipe, and the light pipe is secured directly below the aperture. At this point, the probe tip, the silicon wafer, the light aperture, and the filtered light pipe are aligned. Compressed air is sent through a nozzle on the front of the box until the probe's output voltage

stabilizes. Hence, the air within the box is uniform and the system is ready for testing. A cover is placed over the box to eliminate ambient light. Figure 3.8 shows the measuring system when it is ready for testing.

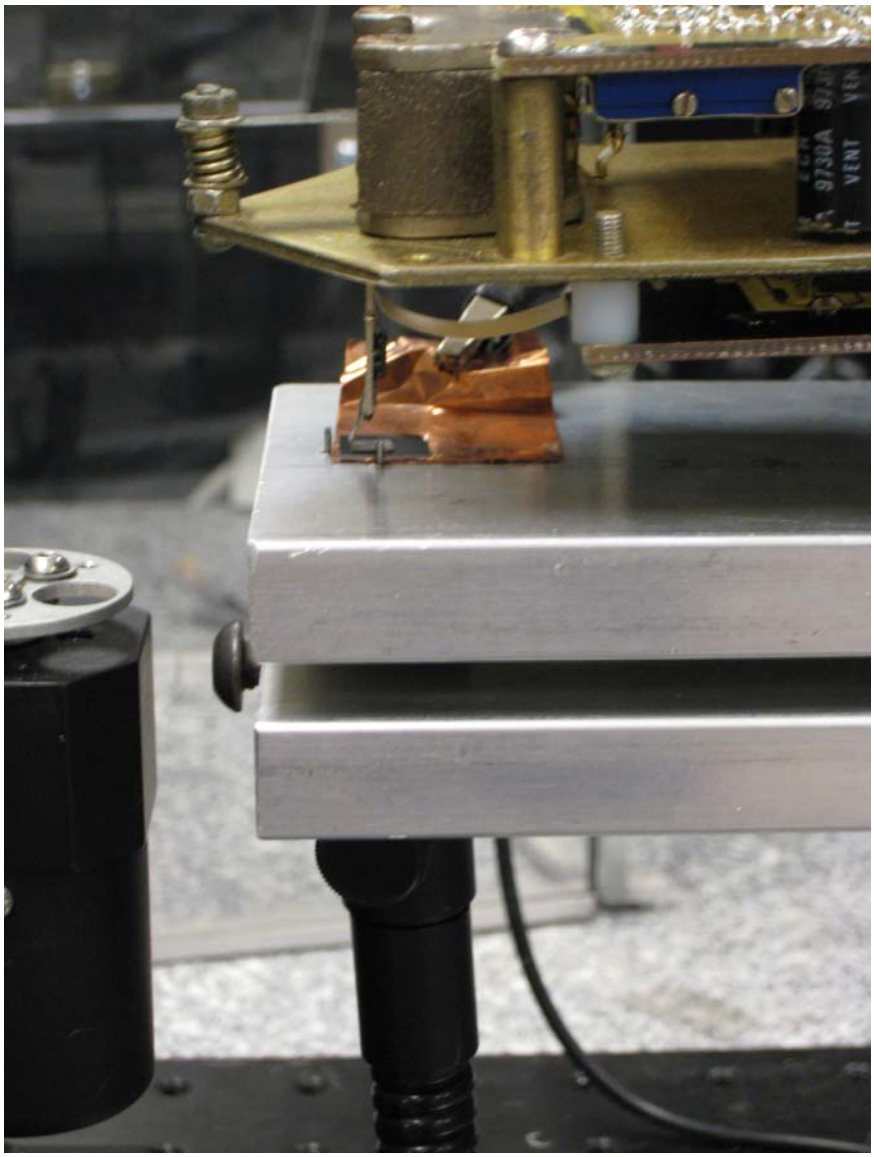

Figure 3.8 Diagram of the measuring device when it is ready for testing. The probe tip, silicon wafer, aperture and light pipe are aligned.

The testing begins by turning on the light source without the light pipe attached to allow the bulb to reach its desired intensity. Once the bulb is fully illuminated, the light

pipe is connected to the light source and data is recorded. While the light pipe is attached, the silicon is illuminated and thus, defined to be in an excited state. After 20 seconds has passed, the light pipe is removed causing the silicon to return to an unexcited state. After an additional 20 seconds, the light pipe is reattached. This process is continued for six to twelve cycles, with each cycle consisting of one excited and one unexcited time period. A 20 second time period is chosen to ensure that the complete transient behavior of the wafer between an unexcited state and a steady-state excited state is recorded. An example of a complete ten cycle test is shown in Figure 3.9.

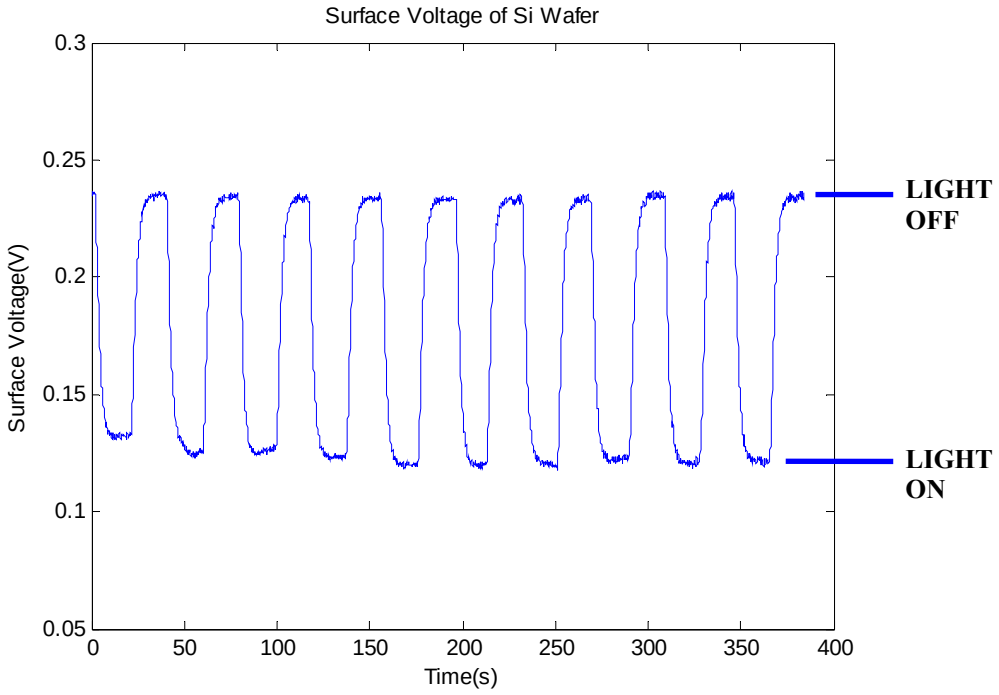

Figure 3.9 Example of the recorded voltage during a ten cycle test.

Two different types of tests based on the properties of the incident light are done on each of the wafers. The first maintains a steady 600 nm wavelength and varies the intensity from 10 % to 100 % of the bulb's maximum intensity in approximately 10 %

increments. For example, a wafer is exposed to six to twelve cycles of light at 10 % intensity while data is recorded. Then the same wafer is exposed to six to twelve cycles of light at 20 % intensity, and so forth until all of the wafers have been exposed to light cycles at all of the intensities. This is appropriately referred to as the intensity test. The other test maintains 100 % light intensity but varies the wavelength from 450 nm to 800 nm in 50 nm increments. The same procedure as the intensity test is followed until all wafers are exposed to all wavelengths of incident light. This is called the wavelength test. After all of data is recorded, it is analyzed with Matlab software.

Qualitative Approach to Modeling

The physical mechanisms occurring in the measuring device parallel those occurring in a MIS-C device. However, the metal probe tip measures potential changes on the silicon wafer's surface instead of actuating the changes. This process can be shown in a series of energy band diagrams in Figure 3.10.

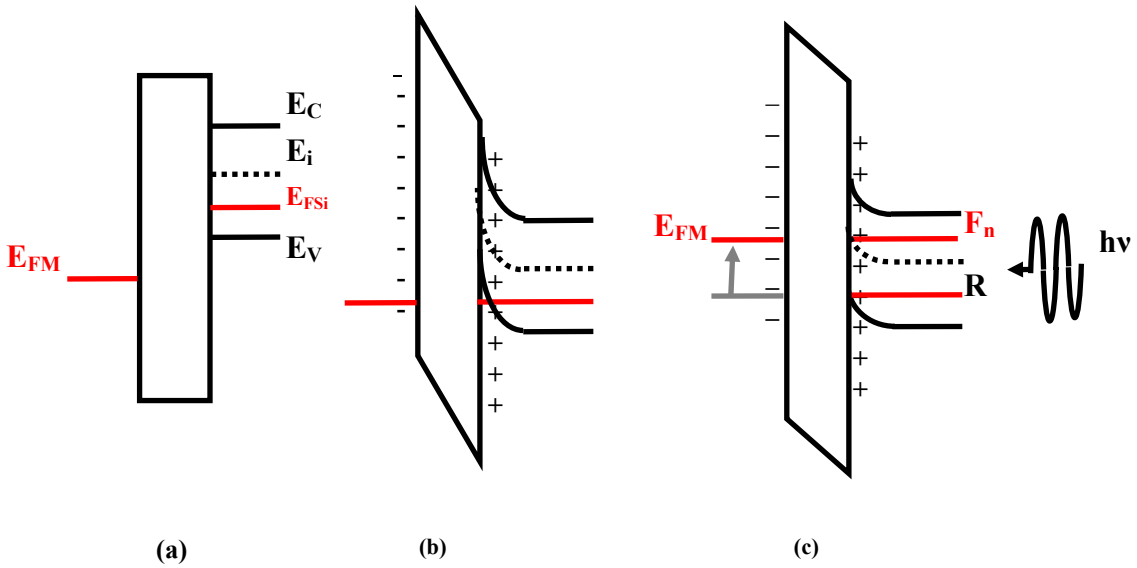

Figure 3.10 Energy Band diagram of the measuring device when (a) disconnected, (b) electrically connected, and (c) electrically connected and excited by incident light.

When a metal and a silicon wafer are electrically connected, Fermi levels will equilibrate. This is labeled as (b) in Figure 3.10. When light is shown on the silicon, decreased band-bending occurs inside the silicon and a quasi-Fermi level is created due to the diffusion of excess electrons. This will cause the Fermi level of the metal to realign with the minority quasi-Fermi level in the silicon. The movement of the Fermi level in the metal will alter the voltage output of the probe. This is labeled as (c) in Figure 3.10.

Quantitative Approach to Modeling

To obtain the governing equations, the device can be modeled as a combination of a MIS-C and a feedback-biasing vibrating Kelvin probe. The diameter of the aperture is much larger than the thickness of the wafer, hence a one-dimensional model is assumed. Because the device is layered by a metal, an insulator and a silicon wafer, the measuring

device operates like a one-dimensional MIS-C. However, the probe tip vibrates above the silicon wafer. Thus, the capacitance changes sinusoidally.

The method of signal generation can be broken into three distinct phenomena occurring inside the silicon wafer: the flow of electrons to form a uniform Fermi level, the absorption of visible light and creation of charged carriers near the rear surface, and the diffusion of the charged carriers to the front surface.

Once a silicon wafer is placed beneath the probe tip, the wafer and the probe tip are electrically connected. Electrons move from the silicon and into the metal probe tip to form a contact potential difference. The value of the contact potential difference can be found from equation 2.1. The energy band diagram is shown in Figure 3.10.

The negative charge developed on the metal probe tip will cause an accumulation of holes at the front surface of the p-type silicon. In accordance with charge neutrality, the magnitude of the positive accumulation charge is equal to the magnitude of the negative charge on the metal probe tip's surface.

$$Q_S = -Q_M = |Q| \tag{3.1}$$

In the above, Q_S is the net positive charge in the silicon's accumulation layer and Q_M is the net negative charge on the metal probe tip's surface. The delta-depletion approximation allows the accumulation of charge in the silicon to be modeled as dirac-delta function [12], in which all charge resides at the front surface of the silicon wafer. The density of holes in the accumulation layer can be found from equation 3.2:

$$p_{Acc} = \frac{Q_S}{|e|} \tag{3.2}$$

As mentioned earlier, the system can be modeled as a parallel plate capacitor. However, air and silicon dioxide separate the probe tip and the silicon and both act as a dielectric. Hence, they can be combined in series to form an equivalent, one-dimensional capacitor.

$$C_{air} = \frac{\varepsilon_o \varepsilon_{air}}{d_{air}} \qquad C_{ox} = \frac{\varepsilon_o \varepsilon_{ox}}{d_{ox}}$$

$$\frac{1}{C_{eq}} = \frac{1}{C_{air}} + \frac{1}{C_{ox}}$$

$$\Rightarrow C_{eq} = \frac{C_{air} C_{ox}}{C_{air} + C_{ox}} = \frac{\varepsilon_0 \varepsilon_{ox} \varepsilon_{air}}{\varepsilon_{air} d_{ox} + \varepsilon_{ox} d_{air}} \tag{3.3}$$

In the above, C_{eq} is the equivalent combined capacitances, C_{ox} is the silicon dioxide capacitance, C_{air} is the air capacitance, ε_{ox} is the dielectric constant of silicon dioxide, ε_{air} is the dielectric constant of air, ε_o is the permittivity of free space, d_{air} is the "thickness" of the air, and d_{ox} is the thickness of the silicon dioxide.

Because of the system's parallel geometry, the charge developed can also be described by equation 2.2. After substitution of the equivalent capacitance into equation 2.2, the charge is shown in equation 3.4.

$$Q_{un} = C_{eq}V_{cpd} = V_{cpd}\left(\frac{C_{air}C_{ox}}{C_{air}+C_{ox}}\right) = V_{cpd}\left(\frac{\varepsilon_0\varepsilon_{ox}\varepsilon_{air}}{\varepsilon_{air}d_{ox}+\varepsilon_{ox}d_{air}}\right) \tag{3.4}$$

In the above, Q_{un} is the charge in the accumulation region of an unexcited silicon wafer. Again, V_{cpd} can be found from equation 2.1.

At this point, the system behaves like a MIS-C with two dielectric materials. In order to find the contact potential difference between the probe tip and the wafer, the probe is vibrated to create a continuously varying, sinusoidal current. The current flowing between the probe tip and wafer can be found by differentiating equation 3.4. All values on the right side are constant except for the "thickness" of the air. The thickness changes sinusoidally with the vibration of the probe tip and can be described by equation 2.6. Hence, the current flowing between the probe tip and the wafer is shown in equation 3.5.

$$i(t) = \frac{\partial Q}{\partial t} = -V_{cpd}\left[\frac{\varepsilon_0\varepsilon_{air}\varepsilon^2{}_{ox}\omega\Delta d\cos(\omega t)}{\left(\varepsilon_{air}d_{ox}+\varepsilon_{ox}\left[d_{avg}+\Delta d\sin(\omega t)\right]\right)^2}\right] \tag{3.5}$$

The current is measured by the vibrating Kelvin probe. A feedback voltage is applied to the probe tip to null the current. The biasing voltage that nulls the current is defined as the output voltage of the probe, V_P.

$$i(t) = \left(V_P - V_{cpd}\right)\left[\frac{\varepsilon_0\varepsilon_{air}\varepsilon^2{}_{ox}\omega\Delta d\cos(\omega t)}{\left(\varepsilon_{air}d_{ox}+\varepsilon_{ox}\left[d_{avg}+\Delta d\sin(\omega t)\right]\right)^2}\right] \tag{3.6}$$

Therefore, the voltage output of the probe is found by setting equation 3.6 equal to zero. The sinusoid will continuously vary with time. Thus, it will have many null points as the current switches direction. Hence, the voltages in the equation are of more importance.

$$i = 0 = V_P - V_{cpd} \tag{3.7}$$
$$\Rightarrow V_P = V_{cpd}$$

The voltage output of the probe is the contact potential difference between the probe tip and the silicon wafer (V_{cpd}).

While the probe tip is vibrating above the front surface of the wafer, the back surface is exposed to steady-state, monochromatic light. This will cause an excess amount of electron-hole pairs inside the silicon near the back surface. Figure 3.11 shows the defined model parameters.

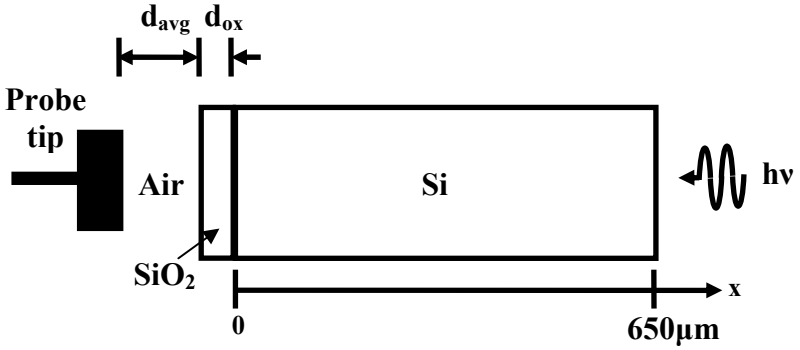

Figure 3.11 Model of the silicon wafer exposed to light.

The number of electron-hole pairs created is dependent on the wavelength and intensity of the light, as well as the wafer's material properties. The absorption of light by a semiconductor was described in detail in the Photovoltaic Effect section. The rate of electron-hole pairs created can be found from equation 2.12.

As mentioned earlier, the amount of electrons and holes created are equal. However, a large number of holes will already exist throughout the wafers due to p-type doping. A condition of low-level injection exists when the number of electron-hole pairs created by absorption of light is many orders of magnitude smaller than the number of majority carriers created from doping. When this condition is met, the number of majority carriers remains the same but the number of minority carriers varies greatly. Therefore, only minority carriers need to be considered. In the silicon wafers tested, low-level injection is assumed for all wavelengths and intensities. Thus, only electrons are considered.

The abundance of electrons near the rear surface causes them to move into the bulk of the silicon to regain equilibrium. Their movement can be described by the minority carrier diffusion equation.

$$\frac{\partial \Delta n}{\partial t} = D_n \frac{\partial^2 \Delta n}{\partial x^2} - \frac{\Delta n}{\tau_n} + G_L \tag{3.8}$$

In the above, Δn is the number of excess electrons and D_n is the diffusion constant for the excess electrons. To simplify the above equation, steady-state is assumed. The simplified equation is shown as equation 3.9.

$$\frac{d^2\Delta n}{dx^2} - \frac{\Delta n}{D_n \tau_n} + \frac{G_L}{D_n} = 0 \tag{3.9}$$

In the above, G_L is described by equation 2.12 fit to the configuration of Figure 3.11.

$$\frac{d^2\Delta n}{dx^2} - \frac{\Delta n}{D_n \tau_n} = \frac{(R-1)N_{ph}\alpha}{D_n} e^{\alpha(x-650\mu m)} \tag{3.10}$$

The minority diffusion equation is reduced to an ordinary differential equation. The variable x, which is the depth into the silicon wafer, is equal to zero at the front surface of the silicon, or the silicon-silicon dioxide interface, as shown in Figure 3.11. A solution for the distribution of excess electrons at steady-state can be found by applying boundary conditions at each surface. The boundary equations are

$$\frac{d\Delta n(x=0)}{dx} = s_{FRONT} \frac{\Delta n(x=0)}{D_n} \tag{3.11a}$$

$$\frac{d\Delta n(x=650\mu m)}{dx} = -s_{REAR} \frac{\Delta n(x=650\mu m)}{D_n} \tag{3.11b}$$

where s_{FRONT} is the recombination velocity at the front surface and s_{REAR} is the recombination velocity at the rear surface. Both equations assume that the change in recombination with respect to depth is proportional to the number of excess electrons at the given surface.

An analytical solution to equation 3.10 with the aid of the given boundary conditions will have the form:

$$\Delta n(x) = A\cosh\left(x/L_n\right) + B\sinh\left(x/L_n\right) + \left[\frac{(1-R)N_{ph}\alpha}{\alpha^2 - \left(1/L_n\right)^2}\right] e^{\alpha(x-650\mu m)} \tag{3.12}$$

$$Ln = \sqrt{D_n \tau_n}$$

where L_n is the electron diffusion length and A and B are constants determined by the boundary equations. Equation 3.10 is solved numerically via Matlab with the aid of the boundary conditions. The "bvp4c" command is used, which is the code for solving boundary value problems by implementing the three-stage Lobatto IIIa formula [26]. All coding can be viewed in Appendix A. The numerical results are used for farther analysis via Matlab.

Equation 3.12 will give the distribution of excess electrons in the silicon wafer. The distribution of excess electrons can be seen in Figures 3.17 and 3.18 in the Simulation Section for varying intensities and wavelengths of incident light, respectively.

It is assumed that excess electrons diffuse to the front surface and recombine with holes in the accumulation layer. Thus, when light is present, the positive charge on the front surface will be reduced. The negative charge due to excess electrons at the front surface during illumination is

$$Q_{\Delta n} = -q\Delta n(x=0) \tag{3.13}$$

The total positive charge at the front surface during illumination, or excitation, is

$$Q_{ex} = Q_{un} - Q_{\Delta n} \tag{3.14}$$

where Q_{un} is the positive charge at the front surface without illumination, described by equation 3.4.

The potential difference during illumination can be found by substituting equation 3.14 into equation 3.4.

$$V_{ex} = Q_{ex}\left(\frac{\varepsilon_{air} d_{ox} + \varepsilon_{ox} d_{air}}{\varepsilon_0 \varepsilon_{ox} \varepsilon_{air}}\right) \tag{3.15}$$

To find the difference between the unexcited and excited potential, a simple subtraction is performed.

$$\Delta V = V_{cpd} - V_{ex} = \left(Q_{un} - Q_{ex}\right)\left(\frac{\varepsilon_{air} d_{ox} + \varepsilon_{ox} d_{air}}{\varepsilon_0 \varepsilon_{ox} \varepsilon_{air}}\right) \tag{3.16}$$

After substituting equation 3.14 into 3.16, the change in potential is

$$\Delta V = Q_{\Delta n}\left(\frac{\varepsilon_{air} d_{ox} + \varepsilon_{ox} d_{air}}{\varepsilon_0 \varepsilon_{ox} \varepsilon_{air}}\right) \tag{3.17}$$

Equation 3.17 describes the front surface potential of the silicon wafer due to the effect of incident light on the rear surface. This is also known as the front surface photovoltage (fSPV). Equation 3.17 states that the fSPV is proportional to the charge associated with the amount of excess electrons at the front surface of the silicon wafer.

The fSPV is easily calculated with parallel-plate capacitor equations due to the delta-depletion approximation, which states that the charge in the accumulation region can be modeled as a dirac-delta function at the silicon's front surface [12]. The model assumes that the only charge in the wafer is at the front surface of the silicon. Thus, it does not account for charge residing in the oxide or at the silicon-silicon dioxide interface. If the charge distribution is more complicated, the potential distribution inside of the silicon wafer can be quantified by solving Poisson's equation with appropriate boundary conditions.

$$\frac{\partial^2 \phi_S}{\partial t^2} = -\frac{\rho}{\varepsilon_S \varepsilon_0} \tag{3.18}$$

In the above, φ_S is the silicon's surface potential, ε_S is the silicon's dielectric constant, and ρ is the charge density.

Simulation

A simulation was designed with Matlab software to test the validity of the model. Before the simulation begins, the user is able to input the properties of a silicon wafer and of the incident light. The program uses this data to predict the difference in voltage between an unexcited and an excited state at the front surface of the silicon, the front

surface photovoltage (fSPV). Graphs of the fSPV for a silicon wafer exposed to light at a range of intensities and wavelengths are shown in Figures 3.12 and 3.13, respectively. The fSPV was calculated only for the discrete intensity and wavelength values used in experimentation. Each tested value is marked with an "X" in Figures 3.12 and 3.13.

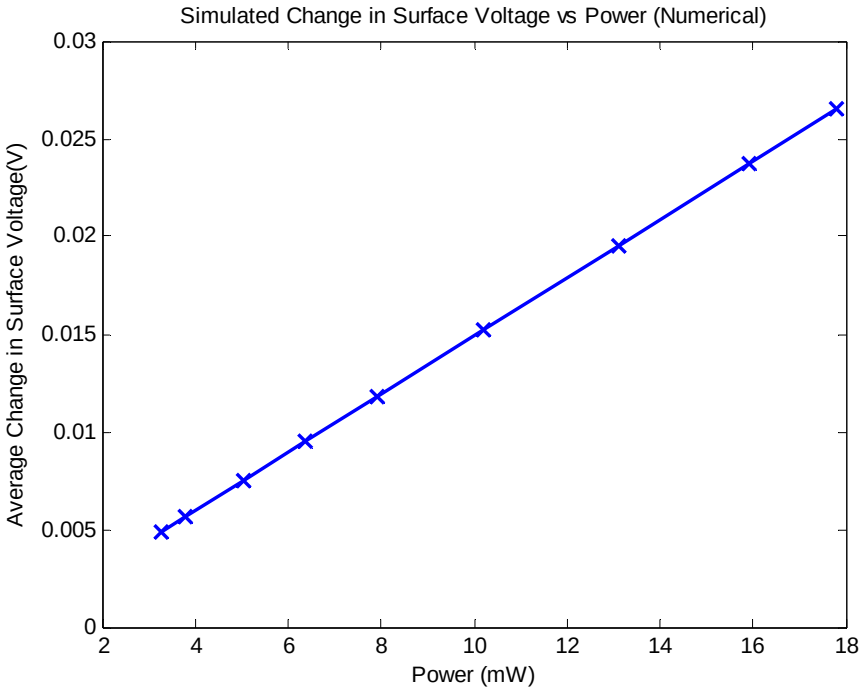

Figure 3.12 Simulated surface potential difference vs. intensity of incident light for a silicon wafer

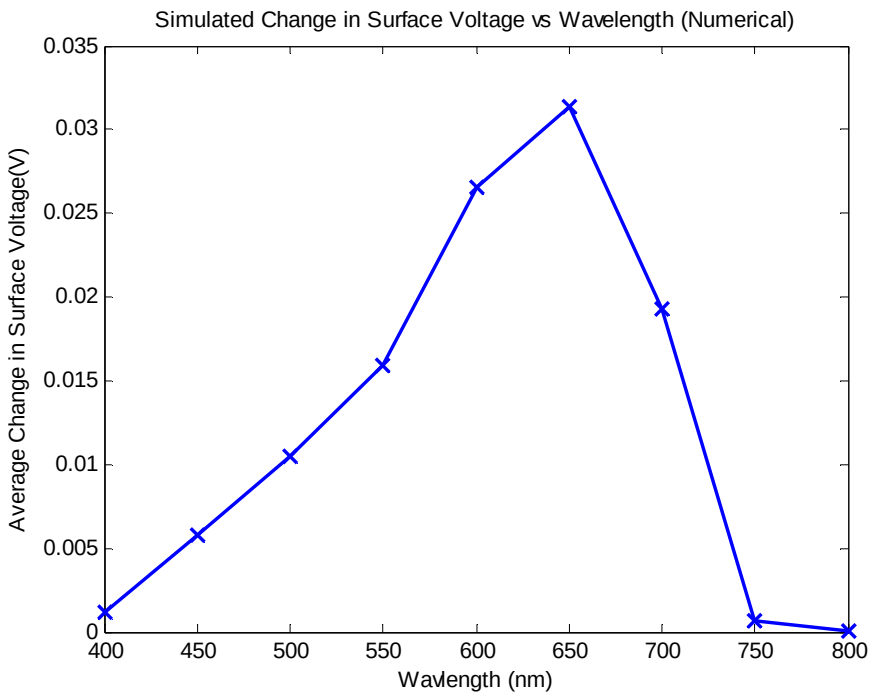

Figure 3.13 Simulated surface potential difference vs. wavelength of incident light for a silicon wafer.

Both graphs show that the fSPV is strongly dependent on the properties of the incident light. The dependence of the fSPV on light intensity, as seen in Figure 3.12, appears linear. Hence, the fSPV for intensities outside of the considered range can be easily extrapolated with the slope and intercept of the line. However, the fSPV's wavelength dependence, as seen in Figure 3.13, appears as a skewed bell curve, much like the power spectrum of the light source, shown in Figure 3.5. Graphs of the simulated fSPV are compared to the experimental results in the next section.

In addition to calculating the voltage difference, the simulation also graphs the distribution of excess electrons within the silicon caused by light absorption. The distribution of excess electrons is found by numerically solving equation 3.10 with

boundary equations 3.11a and 3.11b. Graphs of the excess electrons vs. silicon depth for a range of intensities and wavelengths are shown in Figures 3.14 and 3.15, respectively. The Figures show the electron distribution for a depths between 550 μm and 650 μm into the silicon, whereby x=650 μm is the rear surface. The Figures are included for qualitative purposes only.

The graph of the electron distribution for a range of intensities, Figure 3.14, says a lot about the effect the light intensity has on the wafer. Figure 3.14 shows that the amount of excess electrons increases with increasing intensity. For each intensity, the electron distribution reaches a maximum at approximately 5 μm from the rear surface. This is because the absorption depth is wavelength dependent and all intensities share the same wavelength of 600 nm. After the maximum, the amount of excess electrons decays until the front surface is reached, where x = 0 μm. The amount of excess electrons at the front surface directly manipulates the voltage output of the probe tip. Table 3.2 shows the number of excess electrons near the silicon's front surface and the corresponding simulated fSPV for a range of intensities. The table again illustrates that the amount of excess electrons at the front surface increases with increasing intensity. It also shows that the fSPV increases with increasing amount of excess electrons at the front surface. Hence, a relatively large intensity will have a large fSPV.

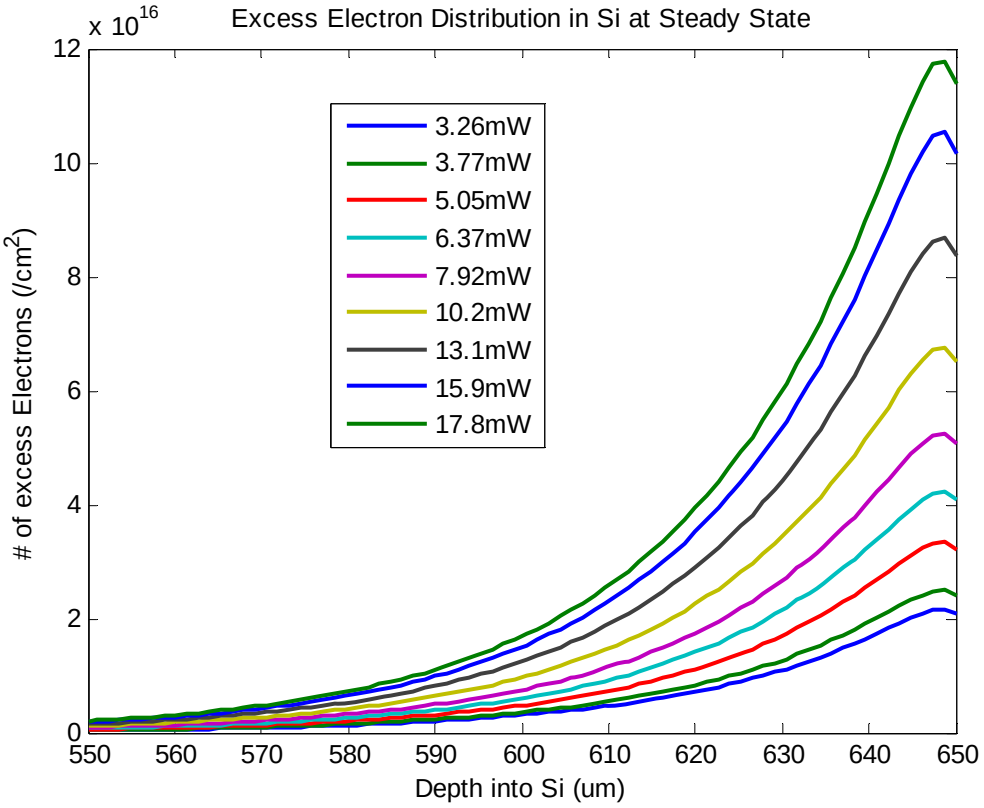

Figure 3.14 Distribution of excess electrons within the silicon wafer exposed incident light with varying intensities.

Table 3.2 Comparison of excess electrons at the front surface and fSPV values for all intensities.

Intensity (mW) **% of max**	Excess electrons at front surface (/cm^2)	fSPV (mV)
3.26 **18**	0.2685 X 10^5	4.9
3.77 **21**	0.3105 X 10^5	5.6
5.05 **28**	0.4159 X 10^5	7.5
6.37 **36**	0.5246 X 10^5	9.5
7.92 **44**	0.6522 X 10^5	11.8
10.2 **57**	0.8400 X 10^5	15.2
13.1 **74**	1.0788 X 10^5	19.5
15.9 **89**	1.3094 X 10^5	23.7
17.2 **100**	1.4659X 10^5	26.5

The graph of the electron distribution for a range of wavelengths, Figure 3.15, says much about the effect the wavelength of light has on the wafer. Figure 3.15 shows that the largest amount of excess electrons is present in the silicon at a wavelength of 650 nm and the least amount is shared at wavelengths of 800 nm and 400 nm. The electron distribution for each wavelength reaches a maximum at different depths in the silicon because the absorption depth is wavelength dependent. As shown in the figure, shorter wavelengths are absorbed, and thus will peak, closer to the surface. Table 3.3 shows the number of excess electrons at the silicon's front surface, at x=0 μm, and the corresponding simulated fSPV for a range of wavelengths. The table again illustrates that the amount of excess electrons at the front surface varies with wavelength. Like Table 3.2, Table 3.3 also shows that the fSPV increases with increasing amount of excess electrons at the front surface.

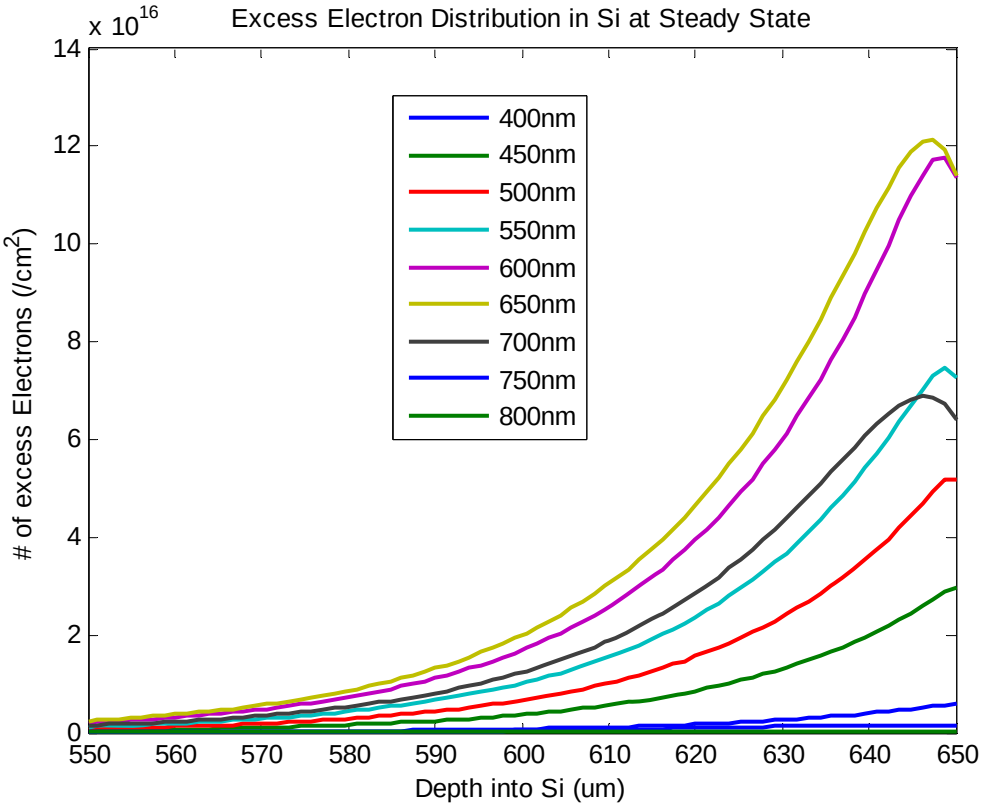

Figure 3.15 Distribution of excess electrons within the silicon wafer exposed incident light with varying wavelengths.

Table 3.3 Comparison of excess electrons at the front surface and fSPV values for all wavelengths.

Wavelength (nm)	Excess electrons at front surface (/cm^2)	fSPV (mV)
400	0.0603 X 10^5	1.1
450	0.3190 X 10^5	5.8
500	0.5788 X 10^5	10.5
550	0.8805 X 10^5	15.9
600	1.4659 X 10^5	26.5
650	1.7337 X 10^5	31.4
700	1.0674 X 10^5	19.3
750	0.0387 X 10^5	0.7
800	0.0053 X 10^5	0.1

Both Table 3.2 and 3.3 clearly show that the fSPV increases with the amount of excess electrons at the front surface. Hence, incident light with properties that facilitate electron creation will have a greater effect on the front surface potential of the silicon wafer.

The simulation also graphs the energy diagrams of the silicon wafer. The quasi-Fermi level for excess electrons (F_N) can be found by solving equation 2.13a. The quasi-Fermi level for holes (F_P) remains the same as the equilibrium Fermi level (E_F) due to low-level injection, as mentioned in the Photovoltaic Effect section. Energy diagrams that include the F_N for a range of intensities and wavelengths are shown in Figures 3.16 and 3.17, respectively. The Figures are shown for qualitative purposes only. Both Figures clearly illustrate that F_N is dependent on the intensity and wavelength of incident light.

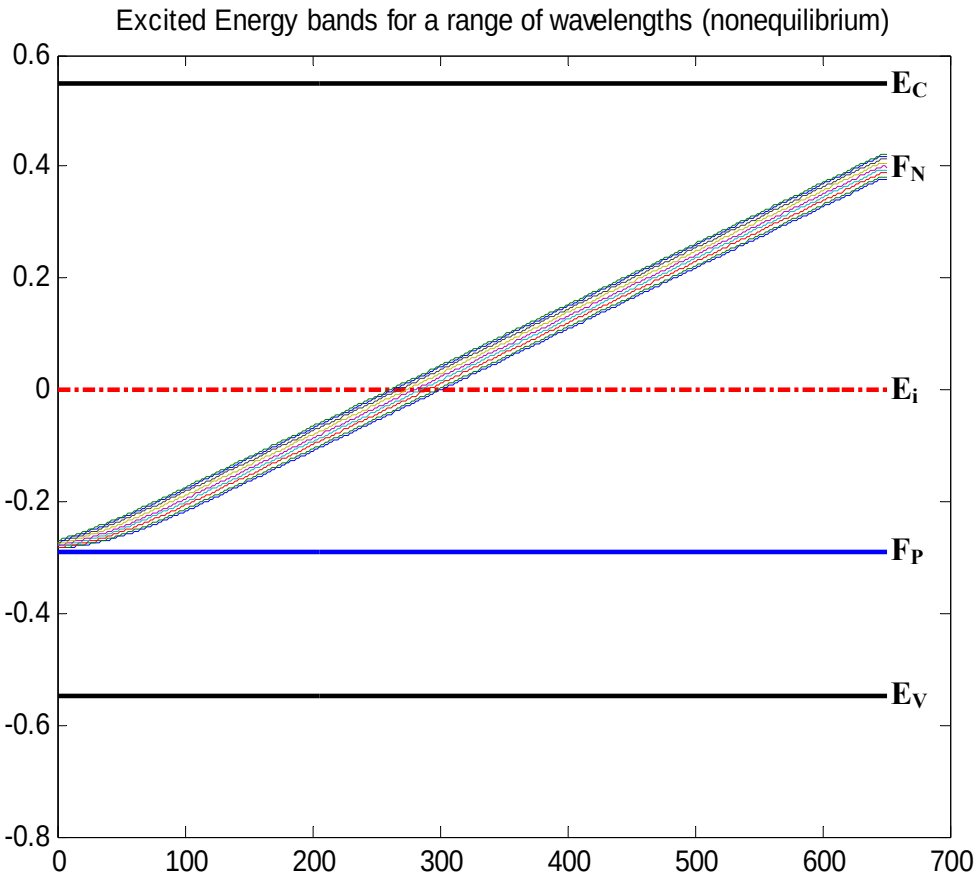

Figure 3.16 Energy diagram of a silicon wafer exposed to light. The electron quasi-Fermi level (F_N) is shown for a range of light intensities.

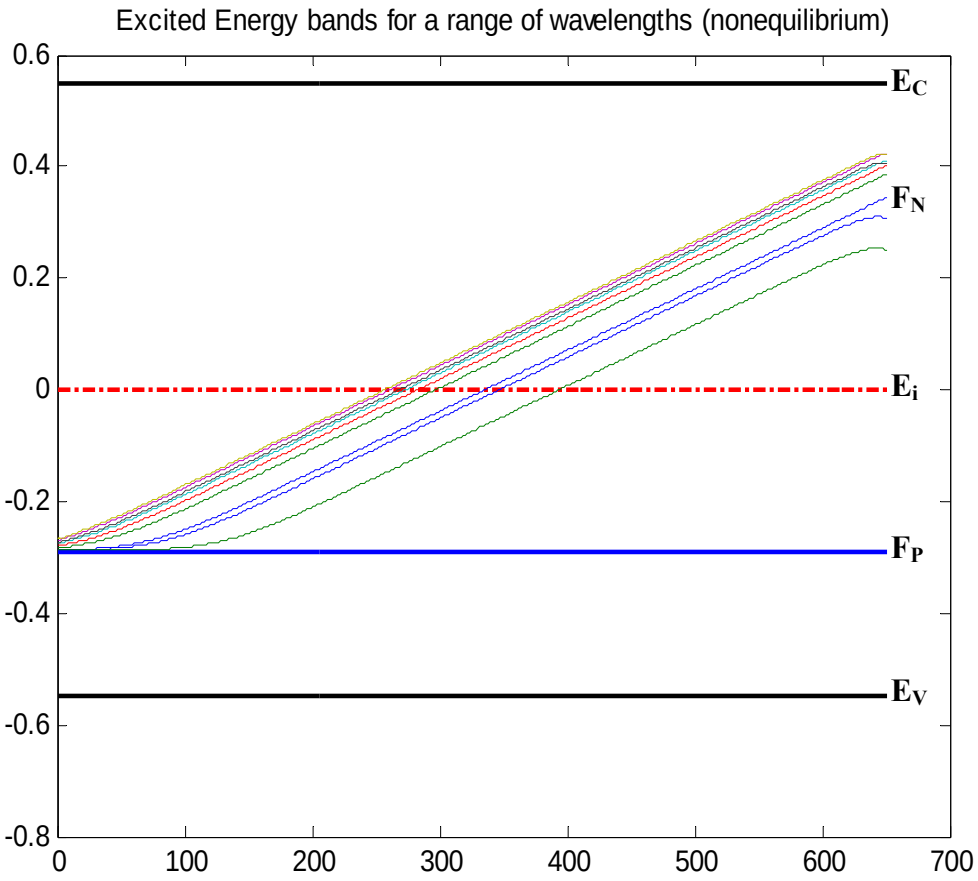

Figure 3.17 Energy diagram of a silicon wafer exposed to light. The electron quasi-Fermi level (F_N) is shown for a range of light wavelengths.

Band-bending is present at the back surface, where x=650 μm, due to the absorption depth of light and the high rear surface recombination velocity. Band-bending of F_N occurs at the front surface only because of high surface recombination velocity. In the bulk of the silicon, F_N is linear with a positive slope. This is a result of the decreased amount of excess electrons towards the front surface of the silicon.

The simulation presents graphical representations of the physical mechanisms occurring within the silicon wafer when exposed to incident light by numerically solving governing equations commonly used to describe silicon devices. All of the graphs

display conditions at steady-state. The simulation can be altered to describe the conditions within any silicon wafer that is tested with the described measuring device.

CHAPTER 4

RESULTS AND ANALYSIS

The Experimental Results and Analysis

Contained in each data curve, i.e. Figure 3.8, is the difference between the average steady-state surface potential measured during illumination and the average surface potential measured without illumination. The potential difference, or front surface photovoltage (fSPV), is found by analyzing each cycle test with Matlab software. The Matlab program averages all of the maximum and minimum voltage values recorded in each light cycle. It then subtracts the average minimum from the average maximum to find the fSPV for a given wafer. As detailed in the last section, each wafer is exposed to six to 12 light cycles of all wavelengths and intensities defined. Figures 4-1 and 4-2 show the fSPV vs. intensity and the fSPV vs. wavelength for each wafer, respectively.

The experimental results show that the fSPV increases with increasing intensity, as illustrated in Figure 4.1.

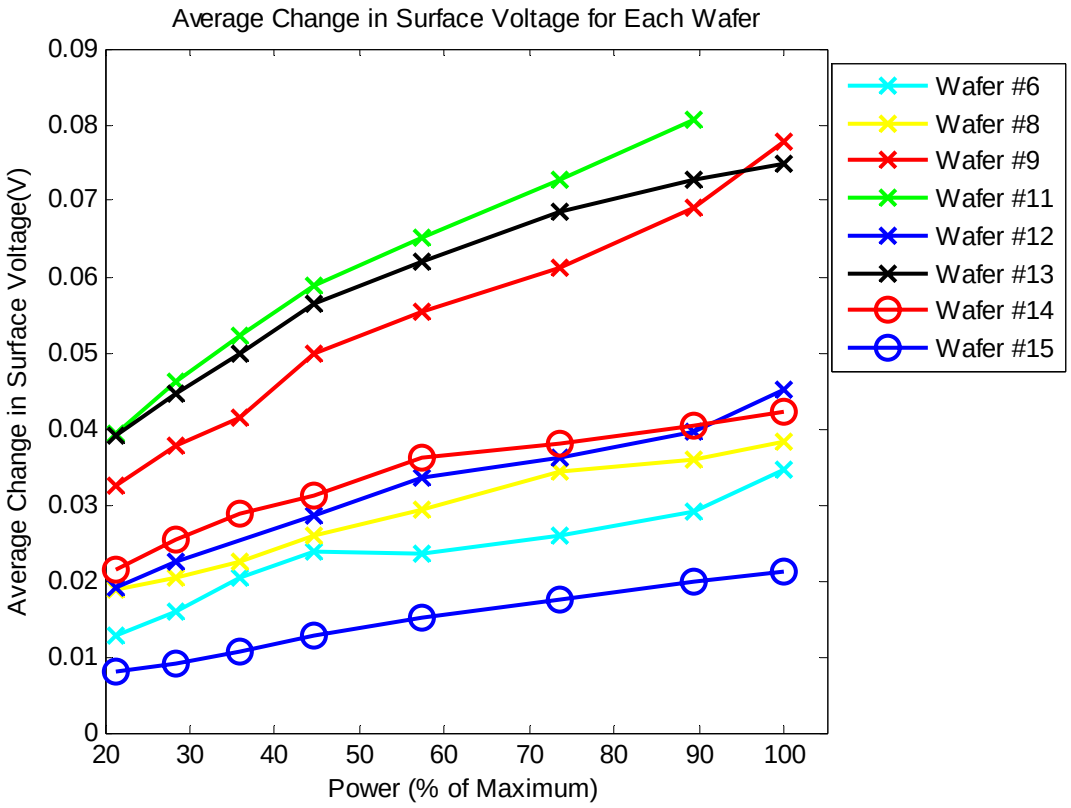

Figure 4.1 The fSPV for a range of light intensities. Wavelength of light is 600nm for all intensities. Maximum Power is 17.8 mW

For each wafer, the smallest fSPV occurred at the lowest intensity, 3.77 mW. In the same respect, the largest fSPV occurred at the highest intensity, 17.8 mW. For all wafers, the fSPV ranged from approximately 8mV at 3.77 mW to approximately 80mV at 17.8 mW.

The experimental results show that the fSPV forms a skewed bell curve with increasing wavelength of incident light, as illustrated in Figure 4.2.

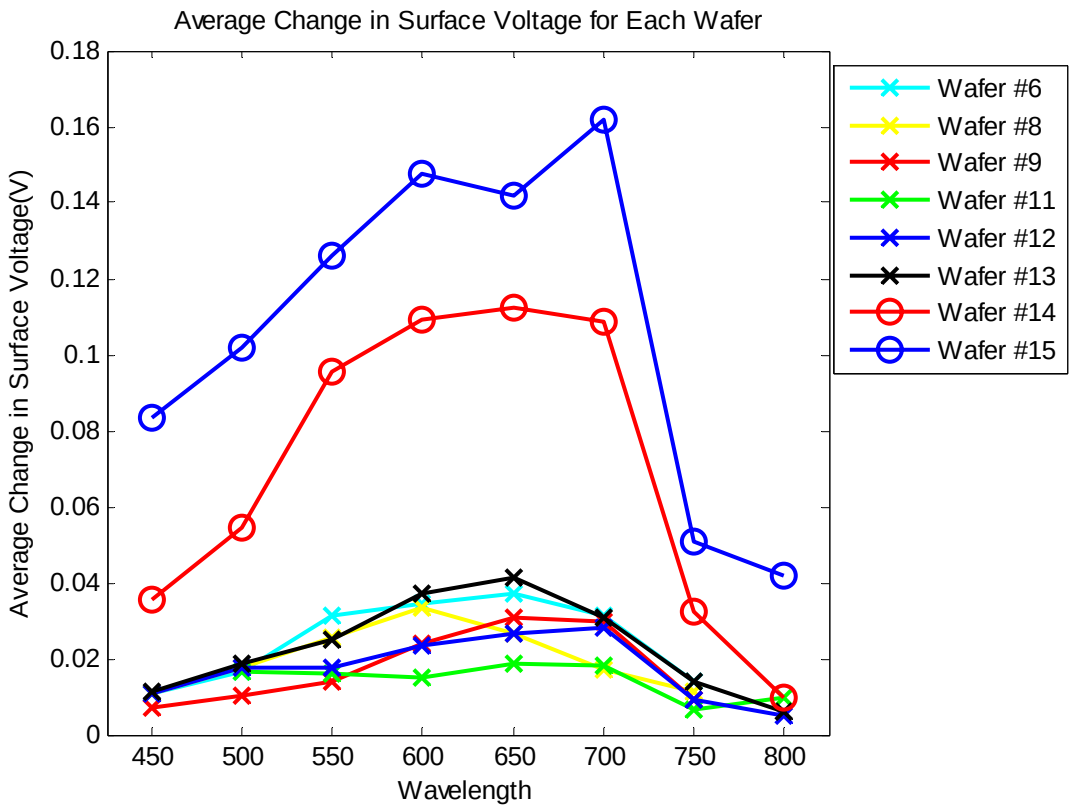

Figure 4.2 The fSPV for a range of light wavelengths. Intensity of light is set at 100% for all wavelengths.

For each wafer, the largest fSPV occurred at mid-range wavelengths, between 600 nm and 700 nm. The smallest fSPV occurred at either 450 nm, the shortest wavelength, or 800 nm, the longest wavelength. For all wafers, the fSPV ranged from approximately 8mV at 800 nm to approximately 165 mV at 700 nm.

The experimental fSPV varies linearly with increased intensity, as does the simulation shown in Figure 3.11. The experimental results obtained during the intensity test were used to determine the approximate values of the front and rear surface recombination rates (s_{FRONT}, s_{REAR}) and the excess electron lifetime (τ_n) of the silicon wafers. All of the silicon wafers were assumed to have uniform surface recombination rates and bulk carrier lifetimes because they were all diced from the same source. The

intensity test results were preferred because of the simple linear relationship. The slope of the line is dependent on the number of excess electrons at the front surface, which, in turn, is dependent on the properties of the silicon wafer. All of the relevant properties were known except for the surface recombination rates and bulk electron lifetime. Those properties can be verified experimentally via the quasi-steady-state photoconductance method [27] however, this method was not available at the time of testing. In this thesis, the surface recombination rates and a bulk electron lifetime were approximated by curve fitting the simulation to the experimental results. The least squares method was used to linearly curve-fit the averaged experimental data. The simulation was matched to the experimental line by adjusting the surface recombination rates and a bulk electron lifetime until the slopes were in agreeance.

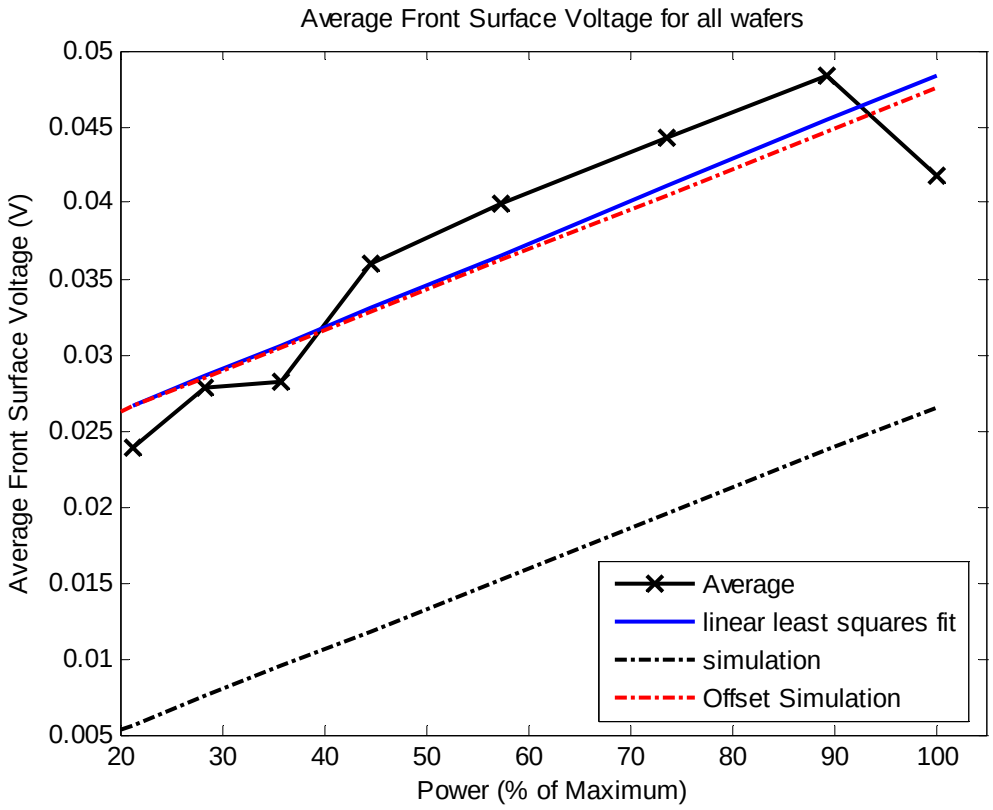

Figure 4.3 The curve fit for experimental data and the coinciding simulation results with and without an offset.

Once the slopes coincided, there was a +22mV offset applied to the simulation, as shown in Figure 4.3. The offset can be attributed to a fixed, positive charge at the silicon/silicon dioxide interface. The effect of a fixed interface charge is discussed in the Effect of Energy Traps section. The values derived for the surface recombination rates (s_{FRONT}=s_{REAR}=18,000cm/s) and the bulk electron lifetime(τ_n=1.6x10^{-7}s) were used in the simulation for both the intensity and wavelength tests, because the identical wafers were used in each test.

The experimental results followed the same trends as the simulation, which allowed for curve-fitting. The curve-fitted simulation values, with and without an offset, are shown with the experimental results in Figures 4.4 and 4.5 for comparison.

Extraneous wavelength curves, marked Wafer #14 and Wafer #15 in Figure 4.2, were omitted from Figure 4.5 and will be discussed in the next paragraph.

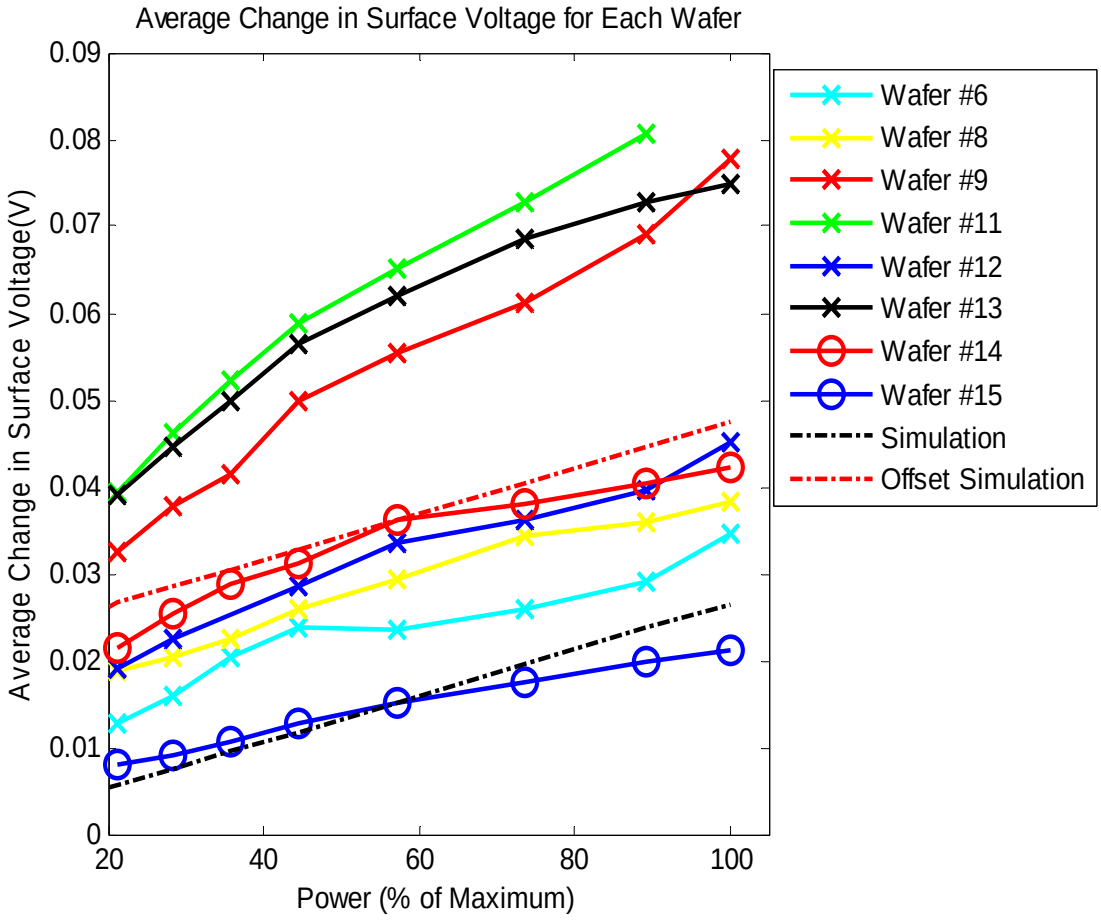

Figure 4.4 The average voltage difference between an excited and an unexcited state for a range of light intensities. Wavelength of light is 600nm for all intensities. Maximum Power is 17.8 mW

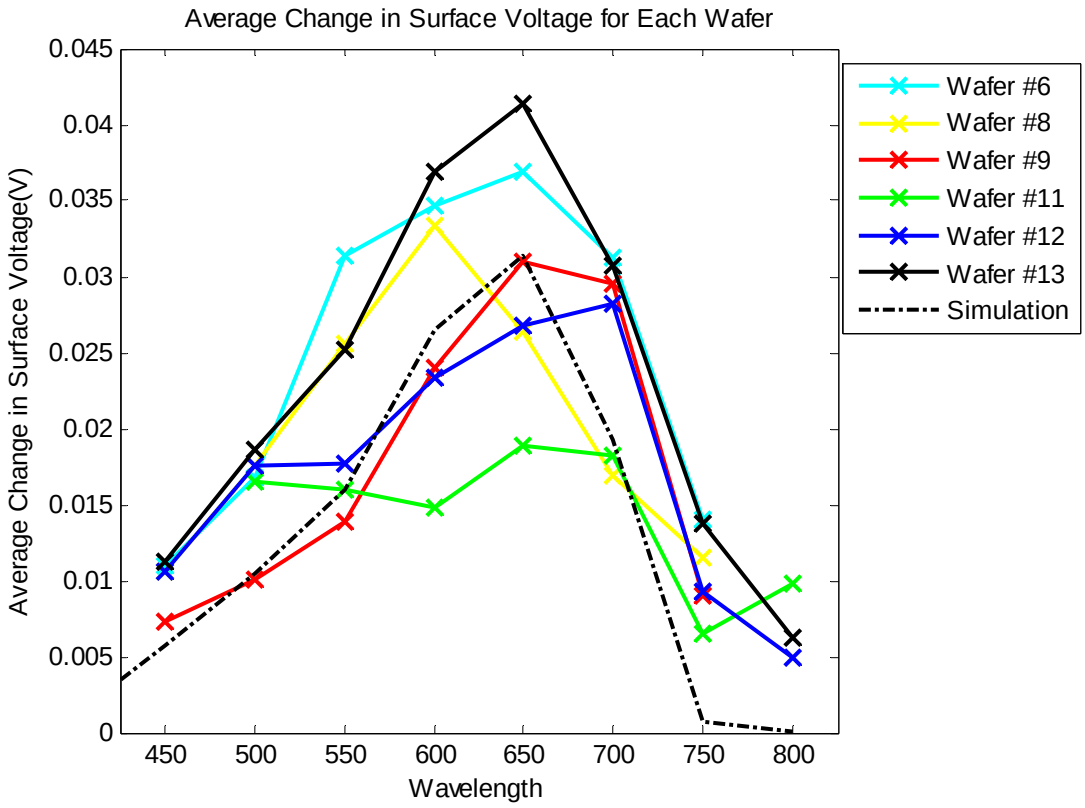

Figure 4.5 The average voltage difference between an excited and an unexcited state for a range of light wavelengths. Light intensity is set to the bulb's maximum value for all wavelengths.

The fSPV increased with increasing intensity and the fSPV formed a skewed bell curve with increasing wavelength. The experimental wavelength curves were more sporadic than the intensity curves. This may be the result the testing procedure during the wavelength test. The isolation box was opened to change the wavelength filter for each wafer. The opening of the box would disturb the ambient environment. During intensity testing the isolation box remained closed. However, as shown in figure 4.5, Wafer #13 was the same shape as the simulation but with an offset of approximately +10 mV. Hence the disturbance appeared to have little effect on Wafer #13.

The experimental fSPV is much larger for Wafers #14 and #15 for all wavelengths tested, as shown in Figure 4.2. This could have been caused by the environmental conditions at the time of testing. Wafers #13 and #14 were both tested when the relative humidity in the testing environment measured approximately 50%. All other wafers were tested in an environment with a relative humidity reading of less than 30%. The potential measured by a Kelvin probe has been shown to increase with humidity [28]. The increased output could be the result of adsorption of condensed water on the wafer's surface. This could be avoided by controlling ambient conditions.

Even though all of the data curves follow the same general trends, no two curves are the same. One of the possible causes of deviation is unsatisfactory wafer handling and storage. The silicon wafers were not kept in clean room quality condition and they were handled with plastic tweezers. The handing and storage of the wafers could have caused local defects, especially on the front and rear surfaces. Defects, such as surface scratches, will cause a change in silicon properties, such as surface recombination velocities and bulk electron lifetime [12]. A detailed description of the effect of defects on surface potential is described in the Effect of Energy Traps section. To avoid defects and ensure consistent results, the wafers should be handled and stored properly.

Another possible cause of error is the ever-changing testing environment. A Plexiglas box surrounding the testing area was used to reduce random fluctuations due to abrupt changes in ambient conditions. However, Kelvin probe measurements are very sensitive to environmental conditions, as mentioned in the Introduction section. Thus, tests should be performed in an ultra-high vacuum (UHV) to maintain a steady environment.

The value derived for the surface recombination rates are considered high ($s_{FRONT}=s_{REAR}=18{,}000$cm/s) and the value obtained for the bulk electron lifetime is considered small ($\tau_n=1.6\text{x}10^{-7}$s). These values infer that the wafers tested had many energy levels in the forbidden band-gap, between the conduction band and the valence band, which would result in poor electronic properties [12]. The allowable energy levels within the forbidden band-gap, or energy traps, are associated with defects within the silicon. The energy trap levels can be quantified by illuminating each surface with light of sub-band-gap energy and observing the fSPV [29]. The energy trap levels or the surface recombination rates and the excess electron lifetime should be verified experimentally.

The Effect of Energy Traps

The effect of energy traps on fSPV measurements has been included in the derivation of the bulk electron recombination rate (equation 2.9b), the surface recombination velocities and the excess electron lifetime. Based on the derived property values, there appears to be a large amount of energy traps present in the wafers [12]. The energy traps can increase the excess electron recombination rate and thus, decrease the effect of incident light. I attribute poor wafer handling and storage to the subpar wafer properties.

Even though energy traps within the silicon have been discussed, a large amount of traps could be present at the silicon/silicon-dioxide interface. Energy traps are present at the interface because of the abrupt termination of the silicon lattice and the subsequent formation of an oxide layer [12]. Thus, oxidation conditions have a strong effect on the

electronic properties at the interface [30]. The energy traps, depending on energy level, can capture nearby charge carriers [12]. The trapped carriers have a relatively long lifetime compared to the excess electrons created by light absorption [31]. Hence, trapped carriers can be modeled as a fixed charge at the interface.

A fixed charge at the silicon/silicon-dioxide interface would significantly change the modeling of the system. The fixed interface charge could be positive or negative depending on the trapping energy level, the density of traps, and the amount of the excess carriers present [12]. Figure 4.3 shows the effect of a fixed interface charge on the band-bending of a p-type silicon wafer.

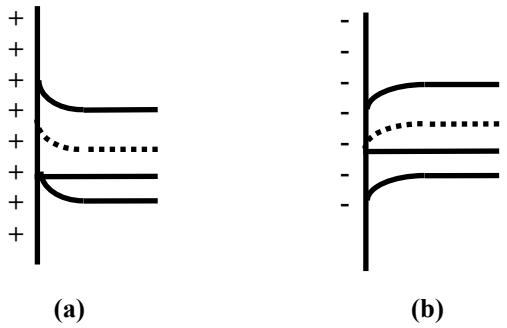

Figure 4.3 Band-bending of a p-type silicon wafer due to a fixed (a) positive or (b) negative silicon-silicon dioxide interface charge.

The consideration of the fixed interface charge farther complicates the model of the measuring system. With a fixed interface charge, the output voltage of the probe takes the form

$$V_p = \frac{Q_F}{C} + V_{cpd} \qquad (4.1)\ [32]$$

where V_p is the voltage output of the probe tip and Q_F is a fixed charge at the silicon /silicon-dioxide interface. Compared to equation 3.7, equation 4.1 includes an extra term representing the effect of the fixed interface charge, $\frac{Q_F}{C}$. The fixed interface charge will produce band-bending near the surface of the silicon. Once light is shown on the rear surface, the band-bending is farther manipulated by excess electrons created from absorbed light.

The constant voltage offset of the simulation, as seen in Figure 4.3, can be attributed to a fixed positive charge at the silicon/silicon-dioxide interface. The fixed interface charge will cause the output voltage of an unexcited wafer to take the form of equation 4.1. The output voltage of an excited wafer is

$$V_p = \frac{Q_F - Q_{\Delta n}}{C} + V_{cpd} \qquad (4.2)$$

where $Q_{\Delta n}$ is the negative charge associated with excess electrons at the front surface of the wafer. The change in the output voltage, or the fSPV, is also described by equation 3.17 which states that the fSPV is due to the amount of excess electrons at the front surface of the wafer. However, the fixed interface charge will induce an electric field near the font surface of the silicon wafer, and thus increase the amount of excess electrons at the front surface.

Using experimental results, the fixed interface charge can be approximated. Equation 4.2 is rearranged to explicitly define the fixed interface charge.

$$Q_F = C\left[V_p - V_{cpd} + \Delta V_{SIM} + 22mV\right] \qquad (4.3)$$

In the above, V_p is the average experimental voltage for an excited wafer exposed to light with a given intensity, V_{cpd} is the contact potential difference described by equation 2.1, ΔV_{SIM} is the simulated fSPV for a given intensity, and 22mV coincides with the simulation offset seen in Figure 4.3. The average fixed interface charge for all tested intensities derived from equation 4.3 is $\frac{Q_F}{q} = 2.4x10^5 / cm^2$. The value is small compared to the fixed interface charge associated with oxide formation, which is in the range of $1x10^{10}$ - $1x10^{12}$ /cm^2 [33]. However, the charge can be attributed to the wafer's exposure to methanol during the cleaning process. In Figure 4.4, a wafer rinsed with methanol has a greater fSPV compared to an unexposed wafer. This result coincides with the accumulation of a positive interface charge. The effect of methanol on the fSPV is discussed in the next section.

The difficulty in using this modeling approach is that the trapping energy levels and the number of interface traps are difficult to quantify. Both values are needed in order to simulate the fixed interface charge.

The Effect of Methanol

Methanol strongly affected the fSPV thus, farther complicating the system. As mentioned in the Experimental Procedure section, each wafer was washed in a methanol bath and subsequently rinsed with DI water to clean the surface. A comparison of the output voltage of a wafer exposed to methanol and one unexposed is shown in Figure 4.4.

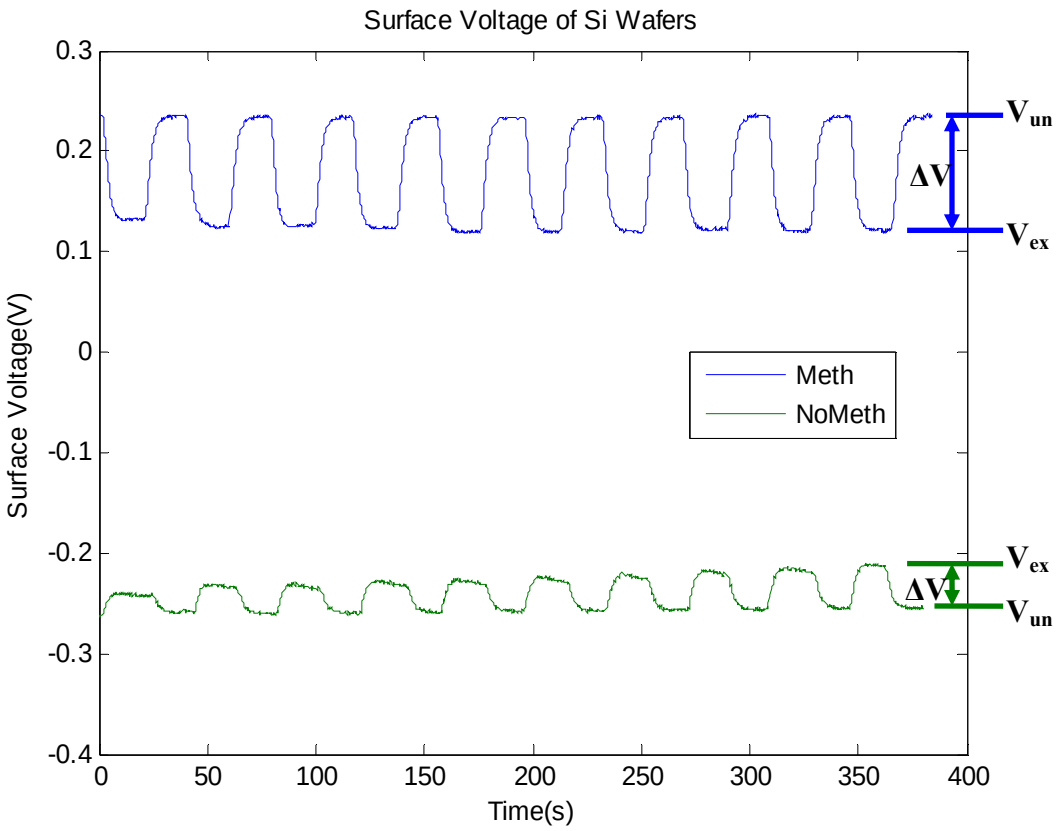

Figure 4.4 The output voltage of a wafer bathed in methanol followed by DI water rinse compared to a wafer not exposed to methanol.

As shown in the Figure, the fSPV, labeled ΔV, of the wafer exposed to methanol was greater than the unexposed wafer. This is in agreement with solar cells immersed in methanol [34]. The unexcited voltage (V_{un}) of the exposed wafer shared the same magnitude as the unexposed wafer, however, it was of opposite sign. This suggests that the wafer accepted electrons from the probe tip when electrically connected, which would induce a state of depletion at the front surface of the silicon wafer instead of accumulation. Hence, Figure 4.4 suggests that the presence of methanol changed the electronic properties at the surface of the wafer. When light was shown on the exposed wafer, the output voltage decreased in magnitude (V_{ex}). This was the same behavior

displayed by the unexposed wafer. Therefore, the magnitude of the output voltage of both wafers was the same, but with opposite signs, and decreased upon illumination.

The transient behavior of both wafers appears to have the same time constant, as shown in Figure 4.4. According to the definition of the excess electron diffusion length (L_n) shown in equation 4.3, an estimate for the amount of time taken for an excess electron to traverse the length of the wafer is τ=120 μs.

$$\tau = \frac{Ln^2}{D_n} \tag{4.4}$$

The slow time constant of 2.3s derived from Figure 4.4 can be attributed to the response of the vibrating Kelvin probe. Hence, the vibrating Kelvin probe used in this thesis is adequate for only steady-state analysis of a silicon wafer exposed to light. If the transient behavior is desired, a vibrating Kelvin probe with a faster response time is needed.

The behavior of the wafer exposed to methanol suggests that the methanol created a fixed positive charge on the wafer's oxide surface, inside the oxide layer, or at the silicon-silicon dioxide interface [16, 23]. It has been shown that the presence of methanol will affect the surface of a silicon wafer with the same orientation as the wafers tested [35, 36]. However, the tested wafers had a native oxide; so a thin layer of silicon dioxide separated the methanol and the silicon. Even though experimental results verify that methanol increases the fSPV, the induced change in surface structure and electronic properties is unknown and needs farther investigation.

CHAPTER 5

CONCLUSION AND FUTURE INVESTIGATION

Conclusion

It has been shown that the front surface potential of a p-type silicon wafer is altered by illuminating the rear surface with monochromatic, visible light. This was verified by monitoring the front surface of a silicon wafer with a vibrating Kelvin probe sensor while illuminating the rear surface. The change in the surface potential between a dark and an illuminated state is dependent on the intensity and wavelength of the light. If the material properties of the silicon wafer and the properties of the light are known, the change in surface voltage can be predicted.

A simple model of the physical mechanisms occurring inside the silicon wafer adequately followed the trends of the experimental outcome, even though all tests were performed under non-ideal experimental conditions. Thus, the output voltage showed robustness to environmental conditions. With this in mind, an optimized and highly predictable output can be achieved with careful control of the testing environment and proper handling of the silicon wafers.

The photovoltage of the silicon wafer is affected by methanol, even after a DI rinse. The exposure to methanol effectively increases the change in the surface potential between a dark and an illuminated state.

Future Investigation

The front surface potential of a silicon wafer is proven to change when the rear surface is exposed to light. Hence, a novel non-vibrating Kelvin probe sensor can be created by combining a typical non-vibrating Kelvin probe, a silicon wafer, and a chopped light source. The current detected by the probe tip is described by

$$i(t) = V\frac{dC}{dt} + C\frac{dV}{dt} \tag{5.1}$$

where V is the potential between the probe tip and the wafer, C is the capacitance of the dielectric, and i is the current in the probe tip. The means of signal generation is the changing potential between the probe tip and the wafer. As shown earlier, the potential changes because the wafer is exposed to rear illumination. If the distance between the probe tip and the wafer is kept constant, the equation simplifies to

$$i = C\frac{d\phi_S}{dt} \tag{5.2}$$

where φ_S is the surface potential of the silicon. If the silicon is of high quality, meaning it has few bulk defects and a thermally grown oxide layer, the transient time constants and the magnitude of the output voltage can be optimized. The frequency of the chopped light can be determined by the silicon wafer's transient response. The probe tip is stationary, so the output will not be affected by interference from an electromechanical drive used for vibration. In addition, the size of the sensor can be reduced because it is comprised of silicon. The advantage of a measuring system with rear illumination is that

the front surface of the wafer, or any fluid placed on the front surface, is unaffected by the illumination.

The proposed system would be effective in measuring any mechanism that alters the work function of silicon. In the Electronic Materials Lab at Georgia Tech, a similar system was used to verify the absorption of motor oil on a silicon wafer's surface [24]. The measuring system, the osCPD device, was explained in the Introduction section. Through use of an alternative form of the Helmholtz equation, equation 5.3, the steady state change in the voltage output between a dark and an illuminated state was related to the fractional surface coverage of the absorbed species [6].

$$\Delta\phi_S = b\theta \tag{5.3}$$

In the above, $\Delta\varphi_S$ is the change in surface voltage between a dark and a light state, b is a proportionality constant found experimentally and θ is the fractional surface coverage of the adsorbate species. In addition, the fractional coverage is related to adsorbate properties through known adsorption isotherms [6]. Theoretically, the type and amount of species adsorbed to the surface of the silicon wafer will affect the output peak-to-peak voltage, or the difference between the maximum and minimum voltage output. Hence, the mere presence of an adsorbate species can be detected by observing the change in steady-state surface potential of an optically stimulated silicon wafer.

APPENDIX A

MATLAB CODING

Intensity Test

```
%this program will break down all vCPD measurements on a given wafer and
%calculate the average change in frontal surface voltage when excited by rear
%illumination.  It will then compare to the Simulation
clf('reset')
clf
clc
clear
b=0;
c=0;
d=0;
e=0;
f=0;
h=0;
i=0;
j=0;
k=0;
%define all files to analyze
files={'022007U06D01600N01BOX','022007U06D02600N01BOX','022007U06D03600N01BOX','022007
U06D04600N01BOX','022007U06070600N01BOX','022007U06080600N01BOX','022007U06090600N01
BOX','022007U06100600N01BOX','022107U07D01600N01BOX','022107U07D02600N01BOX','022107
U07D03600N01BOX','022107U07D04600N01BOX','022107U07070600N01BOX','022107U07080600N0
1BOX','022107U07090600N01BOX','022107U07100600N01BOX','022107U08D01600N01BOX','022107
U08D02600N01BOX','022107U08D03600N01BOX','022107U08D04600N01BOX','022107U08070600N0
1BOX','022107U08080600N01BOX','022107U08090600N01BOX','022107U08100600N01BOX','022607
U09D01600N01','022607U09D02600N01','022607U09D03600N01','022607U09D04600N01','022607U09
070600N01','022607U09080600N01','022607U09090600N01','022607U09100600N01','031407U11D0160
0N01','031407U11D02600N01','031407U11D03600N01','031407U11D04600N01','031407U11070600N01
','031407U11080600N01','031407U11090600N01','031407U12D01600N01','031407U12D02600N01','031
407U12D04600N01','031407U12070600N01','031407U12080600N01','031407U12090600N01','031407U1
2100600N01','031607U13D01600N01','031607U13D02600N01','031607U13D03600N01','031607U13D04
600N01','031607U13070600N01','031607U13080600N01','031607U13090600N01','031607U13100600N0
1','031507U14D01600N01','031507U14D02600N01','031507U14D03600N01','031507U14D04600N01','0
31507U14070600N01','031507U14080600N01','031507U14090600N01','031507U14100600N01','031507
U15D01600N01','031507U15D02600N01','031507U15D03600N01','031507U15D04600N01','031507U15
070600N01','031507U15080600N01','031507U15090600N01','031507U15100600N01'};
AvgDeltaV=zeros(1,length(files));
StanD=zeros(1,length(files));
for a=1:length(files)
   filename=[char(files(a))];
   g=str2num(filename(9));
   l=str2num(filename(8));
   eval(['load ',filename,';'])  %loads the data in 'filename' => VERIFY PATH IS CORRECT!!
   eval(['curve=X',filename,';'])
   time=curve(:,1)';    %defines 'time' as first column of 'filename'
   t=zerostart(time);  %calls function to start time from zero
   Voltage=curve(:,2);
   %plot the raw data
```

```
figure(1)
plot(t,Voltage)
hold all
title('Surface Voltage of Si Wafers')
xlabel('Time(s)')
ylabel('Surface Voltage(V)')
legend(files)
%statistical analysis
z=floor(length(Voltage)/300);  %%determines the number of max/min cycles
deltaV=zeros(1,z);
x=0;
if l==0;
      z=floor(length(Voltage)/400);  %%determines the number of max/min cycles
      deltaV=zeros(1,z);
      x=0;
      for y=1:z
         deltaV(y)=max(Voltage((x+1):(400*y)))-min(Voltage((x+1):(400*y)));  %calculates the delta V
of each cycle
         x=x+400;
      end
elseif l==1;
      z=floor(length(Voltage)/300);  %%determines the number of max/min cycles
      deltaV=zeros(1,z);
      x=0;
      for y=1:z
         deltaV(y)=max(Voltage((x+1):(300*y)))-min(Voltage((x+1):(300*y)));  %calculates the delta V
of each cycle
         x=x+300;
      end
end
if l==0;
     if g==6
         b=b+1;
         AvgDeltaV6(b)=mean(deltaV);   %calculates the average Delta V for a given set of data
         StanD6(b)=std(deltaV);  %calculates the standard deviation of Delta V
         MinV6(b)=min(Voltage);
         MaxV6(b)=max(Voltage);
         StanDV6(b)=std(Voltage);
      end
      if g==7
         c=c+1;
         AvgDeltaV7(c)=mean(deltaV);   %calculates the average Delta V for a given set of data
         StanD7(c)=std(deltaV);  %calculates the standard deviation of Delta V
         MinV7(c)=min(Voltage);
         MaxV7(c)=max(Voltage);
         StanDV7(c)=std(Voltage);
      end
      if g==8
         d=d+1;
         AvgDeltaV8(d)=mean(deltaV);   %calculates the average Delta V for a given set of data
         StanD8(d)=std(deltaV);  %calculates the standard deviation of Delta V
         MinV8(d)=min(Voltage);
         MaxV8(d)=max(Voltage);
         StanDV8(d)=std(Voltage);
      end
      if g==9
```

```
            e=e+1;
            AvgDeltaV9(e)=mean(deltaV);   %calculates the average Delta V for a given set of data
            StanD9(e)=std(deltaV);  %calculates the standard deviation of Delta V
            MinV9(e)=min(Voltage);
            MaxV9(e)=max(Voltage);
            StanDV9(e)=std(Voltage);
        end
    elseif l==1;
        if g==1
            f=f+1;
            AvgDeltaV11(f)=mean(deltaV);   %calculates the average Delta V for a given set of data
            StanD11(f)=std(deltaV);  %calculates the standard deviation of Delta V
            MinV11(f)=min(Voltage);
            MaxV11(f)=max(Voltage);
            StanDV11(f)=std(Voltage);
        end
        if g==2
            h=h+1;
            AvgDeltaV12(h)=mean(deltaV);   %calculates the average Delta V for a given set of data
            StanD12(h)=std(deltaV);  %calculates the standard deviation of Delta V
            MinV12(h)=min(Voltage);
            MaxV12(h)=max(Voltage);
            StanDV12(h)=std(Voltage);
        end
        if g==3
            i=i+1;
            AvgDeltaV13(i)=mean(deltaV);   %calculates the average Delta V for a given set of data
            StanD13(i)=std(deltaV);  %calculates the standard deviation of Delta V
            MinV13(i)=min(Voltage);
            MaxV13(i)=max(Voltage);
            StanDV13(i)=std(Voltage);
        end
        if g==4
            j=j+1;
            AvgDeltaV14(j)=mean(deltaV);   %calculates the average Delta V for a given set of data
            StanD14(j)=std(deltaV);  %calculates the standard deviation of Delta V
            MinV14(j)=min(Voltage);
            MaxV14(j)=max(Voltage);
            StanDV14(j)=std(Voltage);
        end
        if g==5
            k=k+1;
            AvgDeltaV15(k)=mean(deltaV);   %calculates the average Delta V for a given set of data
            StanD15(k)=std(deltaV);  %calculates the standard deviation of Delta V
            MinV15(k)=min(Voltage);
            MaxV15(k)=max(Voltage);
            StanDV15(k)=std(Voltage);
        end
    end
end
    Power=[3.77 5.05 6.37 7.92 10.2 13.1 15.9 17.8]/17.8*100;  %Power measurements at 600nm in
percentage of maximum at 600nm
    Power11=[3.77 5.05 6.37 7.92 10.2 13.1 15.9]/17.8*100;
    Power12=[3.77 5.05 7.92 10.2 13.1 15.9 17.8]/17.8*100;
    %determine change in voltage
    %plot error bars for change in Voltage
```

```
figure(2)
%,Power,AvgDeltaV7,'x-m'
plot(Power,AvgDeltaV6,'x-c',Power,AvgDeltaV8,'x-y',Power,AvgDeltaV9,'x-
r',Power11,AvgDeltaV11,'x-g',Power12,AvgDeltaV12,'x-b',Power,AvgDeltaV13,'x-
k',Power,AvgDeltaV14,'x-r',Power,AvgDeltaV15,'x-b','LineWidth',2,'MarkerSize',10)
hold all
title('Average Change in Surface Voltage for Each Wafer')
xlabel('Power (% of Maximum)')
xlim([20 105])
ylabel('Average Change in Surface Voltage(V)')
legend('Wafer #6','Wafer #8','Wafer #9','Wafer #11','Wafer #12','Wafer #13','Wafer #14','Wafer
#15','Simulation','Offset Simulation')
%plot error bars for change in Voltage
figure(3)
errorbar(Power,AvgDeltaV6,StanD6,'x-c','LineWidth',2,'MarkerSize',10)
legend('Wafer #6','Wafer #8','Wafer #9','Wafer #11','Wafer #12','Wafer #13','Wafer #14','Wafer
#15','Simulation','Offset Simulation')
hold all
figure(3)
%errorbar(Power,AvgDeltaV7,StanD7,'x-m','LineWidth',2,'MarkerSize',10)
%legend('Wafer #6','Wafer #7','Wafer #8','Wafer #9','Wafer #11','Wafer #12','Wafer #13','Wafer
#14','Wafer #15','Simulation')
%hold all
figure(3)
errorbar(Power,AvgDeltaV8,StanD8,'x-y','LineWidth',2,'MarkerSize',10)
legend('Wafer #6','Wafer #8','Wafer #9','Wafer #11','Wafer #12','Wafer #13','Wafer #14','Wafer
#15','Simulation','Offset Simulation')
hold all
figure(3)
errorbar(Power,AvgDeltaV9,StanD9,'x-r','LineWidth',2,'MarkerSize',10)
legend('Wafer #6','Wafer #8','Wafer #9','Wafer #11','Wafer #12','Wafer #13','Wafer #14','Wafer
#15','Simulation','Offset Simulation')
hold all
figure(3)
errorbar(Power11,AvgDeltaV11,StanD11,'x-g','LineWidth',2,'MarkerSize',10)
legend('Wafer #6','Wafer #8','Wafer #9','Wafer #11','Wafer #12','Wafer #13','Wafer #14','Wafer
#15','Simulation','Offset Simulation')
hold all
figure(3)
errorbar(Power12,AvgDeltaV12,StanD12,'x-b','LineWidth',2,'MarkerSize',10)
legend('Wafer #6','Wafer #8','Wafer #9','Wafer #11','Wafer #12','Wafer #13','Wafer #14','Wafer
#15','Simulation','Offset Simulation')
hold all
figure(3)
errorbar(Power,AvgDeltaV13,StanD13,'x-k','LineWidth',2,'MarkerSize',10)
legend('Wafer #6','Wafer #8','Wafer #9','Wafer #11','Wafer #12','Wafer #13','Wafer #14','Wafer
#15','Simulation','Offset Simulation')
hold all
figure(3)
errorbar(Power,AvgDeltaV14,StanD14,'x-r','LineWidth',2,'MarkerSize',10)
legend('Wafer #6','Wafer #8','Wafer #9','Wafer #11','Wafer #12','Wafer #13','Wafer #14','Wafer
#15','Simulation','Offset Simulation')
hold all
figure(3)
errorbar(Power,AvgDeltaV15,StanD15,'x-b','LineWidth',2,'MarkerSize',10)
```

```
    legend('Wafer #6','Wafer #8','Wafer #9','Wafer #11','Wafer #12','Wafer #13','Wafer #14','Wafer
#15','Simulation','Offset Simulation')
    hold all
    title('Average Change in Surface Voltage for Each Wafer')
    xlabel('Power (% of Maximum)')
    ylabel('Average Change in Surface Voltage(V)')
    xlim([20 105])
    %determine drift of signal
    figure(4)
    %,Power,MinV7,'x-m'
    plot(Power,MinV6,'x-c',Power,MinV8,'x-y',Power,MinV9,'x-r',Power11,MinV11,'x-
g',Power12,MinV12,'x-b',Power,MinV13,'x-k',Power,MinV14,'x-r',Power,MinV15,'x-
b','LineWidth',2,'MarkerSize',10)
    legend('Min Wafer #6','Min Wafer #8','Min Wafer #9','Min Wafer #11','Min Wafer #12','Min Wafer
#13','Min Wafer #14','Min Wafer #15','Max Wafer #6','Max Wafer #8','Max Wafer #9','Max Wafer
#11','Max Wafer #12','Max Wafer #13','Max Wafer #14','Max Wafer #15')
    hold all
    figure(4)
    %,Power,MaxV7,'x--m'
    plot(Power,MaxV6,'x--c',Power,MaxV8,'x--y',Power,MaxV9,'x--r',Power11,MaxV11,'x--
g',Power12,MaxV12,'x--b',Power,MaxV13,'x--k',Power,MaxV14,'x--r',Power,MaxV15,'x--
b','LineWidth',2,'MarkerSize',10)
    legend('Min Wafer #6','Min Wafer #8','Min Wafer #9','Min Wafer #11','Min Wafer #12','Min Wafer
#13','Min Wafer #14','Min Wafer #15','Max Wafer #6','Max Wafer #8','Max Wafer #9','Max Wafer
#11','Max Wafer #12','Max Wafer #13','Max Wafer #14','Max Wafer #15')
    title('Minimum and Maximum Surface Voltage for Each Wafer to Determine Drift')
    xlabel('Power (% of Maximum)')
    ylabel('Min/Max Surface Voltage(V)')
    xlim([20 105])
%%%%Simulate%%%%
%Range of parameters
P= [3.26 3.77 5.05 6.37 7.92 10.2 13.1 15.9 17.8]; %Power (mW)
lamda=600*ones(1,length(P));  %wavelength of light(nm)
lamda=lamda/10^(9); %wavelength of light(m)
alpha=4.5*10^3*ones(1,length(P));  %Si light absorption coefficent,Figure 3.20 (dependent on
wavelngth)(/cm)
  %Define all constants
  h=4.136*10^(-15); %Planck's constant (eV*s)
  c=2.99*10^8; %speed of light in a vacuum (m/s)
  k=8.617*10^(-5); %Boltzman constant (eV/K)
  T=300;  %Temperature (K)
  q=1.602*10^(-19);  %unit of photon charge (C)
  einstein=0.0259;  %'Einstein constant', kT/q, at 300K (V)
  Epsilon0=8.8542*10^(-12)/100;  %permittivity of free space (C^2/J*cm)
  ni=1*10^(10); %intrinsic carrier concentration for Si at 300K (Fig 2.20)(/cm^3)
  Ks=11.8;  %Si dielectric Constant
  Ko=3.9;  %oxide dielectric Constant
  Ka=1; %air dielectric Constant
  Na=7*10^14;  %doping, Figure 3.8 (/cm^3) (considered not heavily doped!)
  EpsilonS=Ks*Epsilon0;  %permittivity of Si (C^2/J*cm)
  EpsilonOx=Ko*Epsilon0;  %permittivity of oxide (C^2/J*cm)
  chi=4.03; %intrinsic electron affinity work function (eV)
  EiEf=k*T*log(Na/ni); %difference between intrinsic Fermi level and doped Fermi level of Si  (eV)
  PhiSi=chi+EiEf+(1.01/2); %silicon work function (eV)
  PhiNi=5.01;  %Nickel work function (eV)
  Vcpd=((PhiNi-PhiSi)/q)*q; %contact potential difference between bulk Si and probe tip (V)
```

```
   B=2*10^(-15);  %material constant in Si (cm^3/s)
   %Define Si Wafer Properties
   rho=20;  %resistivity (Ohm/cm)
   Mup=459;  %Majority Carrier Mobility, Figure 3.5 (cm^2/(V-sec))
   Mun=1350;  %Minority Carrier Mobility, Figure 3.5 (cm^2/(V-sec))
   po=Na;  %majority carriers (/cm^3)
   no=(ni)^2/Na;  %minority carriers (/cm^3)
   Tauln=1.6*10^(-7);  %carrier lifetime (sec)  (Verify experimentally)
   Dn=einstein*Mun;  %diffusion constant related to Mu through Einstein Rel (cm^2/(sec))
   sFr=18000;  %front surface recombination velocity (cm/s)
   sBk=sFr;    %back surface recombination velocity (cm/s)
   Ln=sqrt(Dn*Tauln);%Minority Carrier Diffusion Lengths (cm);
   r=1;  %length of side  of aperture (cm)
   A=pi*r^2; %planar area of aperture (cm^2)
   dox=(47+74+79)/3*(1*10^(-8));  %average oxide thickness (cm)
   dair=1/10;  %average fly height(cm)
   C=((Epsilon0)*Ko*Ka)/(((dox)*Ka)+((dair)*Ko)); %capacitance of air and oxide layer (F/cm=C^2/Jcm)
   Q=C*Vcpd; %charge on the capacitor in the dark (C/cm)
for i=1:length(P)
   I=(P(i)/(1*10^3))/A;  %Intensity of light (W/cm^2)
   R=.32;
   %R=0.3214+.03565/(lamdaMicro(i))-.03149/(lamdaMicro(i))^2;  %fraction of light reflected at the
surface
   Eph=h*c/(lamda(i)); %energy of a photon (eV)
   Nph=(I/(Eph*q)); %photon density per sec (photons/(cm^2*sec))
   alpha1=alpha(i);
   %Numerically find the number of excess electrons created by light
   %Call function to solve minority carrier diffusion Equation (BVP)
   NumDeltaN=MinorityCarriersSchroder(Ln,Dn,Nph,alpha1,R,sFr,sBk); %distribution of the # of excess
electrons created (electron/um^2)
   NumDeltaN=NumDeltaN*(1*10^4)^2; %distribution of the # of excess electrons created
(electron/cm^2)
   NumDeltaNFr(i)=NumDeltaN(1); %# of excess electrons created at the surface (electron/cm^2)
   %%%Voltage Analysis%%%
   Qel=-NumDeltaNFr(i)*q; %amount of charge on the surface due to excess electrons (C/cm^2)
   Qex=Q+Qel;  %total amount of charge on the surface when light is present(C/cm^2)
   Vun=Vcpd; %surface voltage unexcited
   Vex=Qex/C; %surface voltage unexcited
   DeltaVSurface(i)=Vun-Vex;
end
%%%Match simulation to experimental data%%%
   AvgDeltaV11=[AvgDeltaV11 0];
   AvgDeltaV12=[AvgDeltaV12(1) AvgDeltaV12(2) 0 AvgDeltaV12(3) AvgDeltaV12(4) AvgDeltaV12(5)
AvgDeltaV12(6) AvgDeltaV12(7)];
   AvgDeltaV=[AvgDeltaV6; AvgDeltaV8; AvgDeltaV9; AvgDeltaV11; AvgDeltaV12; AvgDeltaV13;
AvgDeltaV14; AvgDeltaV15];
   AvgfSPV=mean(AvgDeltaV); %finds average value at each intensity
LinearCoeffExp=polyfit(Power,AvgfSPV,1); %Finds coefficients of the line that linearly fits the AvgfSPV
data
LiearfSPV=Power.*LinearCoeffExp(1)+LinearCoeffExp(2);
Offset=LiearfSPV(1)-DeltaVSurface(2);
DeltaVSurface2=DeltaVSurface+Offset;
%end
%plot results
P= [3.26 3.77 5.05 6.37 7.92 10.2 13.1 15.9 17.8]/17.8*100;
figure(2)
```

```
plot(P,DeltaVSurface,'k-.','LineWidth',2,'MarkerSize',10)
hold all
legend('Wafer #6','Wafer #8','Wafer #9','Wafer #11','Wafer #12','Wafer #13','Wafer #14','Wafer
#15','Simulation','Offset Simulation')
figure(3)
plot(P,DeltaVSurface,'k-.','LineWidth',2,'MarkerSize',10)
hold all
legend('Wafer #6','Wafer #8','Wafer #9','Wafer #11','Wafer #12','Wafer #13','Wafer #14','Wafer
#15','Simulation','Offset Simulation')
figure(2)
plot(P,DeltaVSurface2,'r-.','LineWidth',2,'MarkerSize',10)
hold all
legend('Wafer #6','Wafer #8','Wafer #9','Wafer #11','Wafer #12','Wafer #13','Wafer #14','Wafer
#15','Simulation','Offset Simulation')
figure(3)
plot(P,DeltaVSurface2,'r-.','LineWidth',2,'MarkerSize',10)
hold all
legend('Wafer #6','Wafer #8','Wafer #9','Wafer #11','Wafer #12','Wafer #13','Wafer #14','Wafer
#15','Simulation','Offset Simulation')
figure(5)
plot(Power,AvgfSPV,'xk-','LineWidth',2,'MarkerSize',10)%plots averaged value for each intensity for all
wavelengths
hold all
title('Average Front Surface Voltage for all wafers')
xlabel('Power (% of Maximum)')
xlim([20 105])
ylabel('Average Front Surface Voltage (V)')
legend('Average','linear least squares fit','simulation')
figure(5)
plot(Power,LiearfSPV,'b-','LineWidth',2,'MarkerSize',10)
legend('Average','linear least squares fit','simulation','Offset Simulation')
hold all
figure(5)
plot(P,DeltaVSurface,'k-.','LineWidth',2,'MarkerSize',10)
legend('Average','linear least squares fit','simulation','Offset Simulation')
hold all
figure(5)
plot(P,DeltaVSurface2,'r-.','LineWidth',2,'MarkerSize',10)
legend('Average','linear least squares fit','simulation','Offset Simulation')
hold all
%%%Determine fixed interface charge%%%
VexQ=Vex(2:end);
for i=1:length(AvgfSPV)
   Qf(i)=(C*(VexQ(i)-Vcpd+AvgfSPV(i)+0.022))/q;
end
Qfavg=mean(Qf)
```

Wavelength Test

```
%this program will break down all vCPD measurements on a given wafer and
%calculate the average change in frontal surface voltage when excited by rear
%illumination
clf('reset')
clf
```

```
clc
clear
b=0;
c=0;
d=0;
e=0;
f=0;
h=0;
i=0;
j=0;
k=0;
%define all files to analyze
files={'022207U06100450N01','022207U06100500N01','022207U06100550N01','022207U06100600N01','
022207U06100650N01','022207U06100700N01','022207U06100750N01','022307U07100450N01','02230
7U07100500N01','022307U07100550N01','022307U07100600N01','022307U07100650N01','022307U071
00700N01','022307U07100750N01','022307U08100450N01','022307U08100500N01','022307U08100550
N01','022307U08100600N01','022307U08100650N01','022307U08100700N01','022307U08100750N01','0
22307U09100450N01','022307U09100500N01','022307U09100550N01','022307U09100600N01','022307
U09100650N01','022307U09100700N01','022307U09100750N01','031607U11100500N01','031607U1110
0550N01','031607U11100600N01','031607U11100650N01','031607U11100700N01','031607U11100750N
01','031607U11100800N01','031607U12100450N01','031607U12100500N01','031607U12100550N01','03
1607U12100600N01','031607U12100650N01','031607U12100700N01','031607U12100750N01','031607U
12100800N01','031907U13100450N01','031907U13100500N01','031907U13100550N01','031907U13100
600N01','031907U13100650N01','031907U13100700N01','031907U13100750N01','031907U13100800N0
1','031907U14100450N01','031907U14100500N01','031907U14100550N01','031907U14100600N01','031
907U14100650N01','031907U14100700N01','031907U14100750N01','031907U14100800N01','031907U1
5100450N01','031907U15100500N01','031907U15100550N01','031907U15100600N01','031907U151006
50N01','031907U15100700N01','031907U15100750N01','031907U15100800N01'};
AvgDeltaV=zeros(1,length(files));
StanD=zeros(1,length(files));
for a=1:length(files)
   filename=[char(files(a))];
   g=str2num(filename(9));
   l=str2num(filename(8));
   eval(['load ',filename,';'])  %loads the data in 'filename' => VERIFY PATH IS CORRECT!!
   eval(['curve=X',filename,';'])
   time=curve(:,1)';    %defines 'time' as first column of 'filename'
   t=zerostart(time);  %calls function to start time from zero
   Voltage=curve(:,2);
   %plot the raw data
   figure(1)
   plot(t,Voltage)
   hold all
   title('Surface Voltage of Si Wafers')
   xlabel('Time(s)')
   ylabel('Surface Voltage(V)')
   legend(files)
   %statistical analysis
   if l==0;
        z=floor(length(Voltage)/400);  %%determines the number of max/min cycles
        deltaV=zeros(1,z);
        x=0;
        for y=1:z
           deltaV(y)=max(Voltage((x+1):(400*y)))-min(Voltage((x+1):(400*y)));   %calculates the delta V
of each cycle
           x=x+400;
```

```
        end
    elseif l==1;
        z=floor(length(Voltage)/300);  %%determines the number of max/min cycles
        deltaV=zeros(1,z);
        x=0;
        for y=1:z
            deltaV(y)=max(Voltage((x+1):(300*y)))-min(Voltage((x+1):(300*y)));   %calculates the delta V
of each cycle
            x=x+300;
        end
    end
    if l==0;
        if g==6
            b=b+1;
            AvgDeltaV6(b)=mean(deltaV);   %calculates the average Delta V for a given set of data
            StanD6(b)=std(deltaV);  %calculates the standard deviation of Delta V
            MinV6(b)=min(Voltage);
            MaxV6(b)=max(Voltage);
            StanDV6(b)=std(Voltage);
        end
        if g==7
            c=c+1;
            AvgDeltaV7(c)=mean(deltaV);   %calculates the average Delta V for a given set of data
            StanD7(c)=std(deltaV);  %calculates the standard deviation of Delta V
            MinV7(c)=min(Voltage);
            MaxV7(c)=max(Voltage);
            StanDV7(c)=std(Voltage);
        end
        if g==8
            d=d+1;
            AvgDeltaV8(d)=mean(deltaV);   %calculates the average Delta V for a given set of data
            StanD8(d)=std(deltaV);  %calculates the standard deviation of Delta V
            MinV8(d)=min(Voltage);
            MaxV8(d)=max(Voltage);
            StanDV8(d)=std(Voltage);
        end
        if g==9
            e=e+1;
            AvgDeltaV9(e)=mean(deltaV);   %calculates the average Delta V for a given set of data
            StanD9(e)=std(deltaV);  %calculates the standard deviation of Delta V
            MinV9(e)=min(Voltage);
            MaxV9(e)=max(Voltage);
            StanDV9(e)=std(Voltage);
        end
    elseif l==1;
        if g==1
            f=f+1;
            AvgDeltaV11(f)=mean(deltaV);   %calculates the average Delta V for a given set of data
            StanD11(f)=std(deltaV);  %calculates the standard deviation of Delta V
            MinV11(f)=min(Voltage);
            MaxV11(f)=max(Voltage);
            StanDV11(f)=std(Voltage);
        end
        if g==2
            h=h+1;
            AvgDeltaV12(h)=mean(deltaV);   %calculates the average Delta V for a given set of data
```

```
            StanD12(h)=std(deltaV);  %calculates the standard deviation of Delta V
            MinV12(h)=min(Voltage);
            MaxV12(h)=max(Voltage);
            StanDV12(h)=std(Voltage);
        end
        if g==3
            i=i+1;
            AvgDeltaV13(i)=mean(deltaV);   %calculates the average Delta V for a given set of data
            StanD13(i)=std(deltaV);  %calculates the standard deviation of Delta V
            MinV13(i)=min(Voltage);
            MaxV13(i)=max(Voltage);
            StanDV13(i)=std(Voltage);
        end
        if g==4
            j=j+1;
            AvgDeltaV14(j)=mean(deltaV);   %calculates the average Delta V for a given set of data
            StanD14(j)=std(deltaV);  %calculates the standard deviation of Delta V
            MinV14(j)=min(Voltage);
            MaxV14(j)=max(Voltage);
            StanDV14(j)=std(Voltage);
        end
        if g==5
            k=k+1;
            AvgDeltaV15(k)=mean(deltaV);   %calculates the average Delta V for a given set of data
            StanD15(k)=std(deltaV);  %calculates the standard deviation of Delta V
            MinV15(k)=min(Voltage);
            MaxV15(k)=max(Voltage);
            StanDV15(k)=std(Voltage);
        end
    end
end
    Wavelength1=[450:50:750];
    Wavelength=[450:50:800];
    Wavelength11=[500:50:800];
    %determine change in voltage
    figure(2)
    plot(Wavelength1,AvgDeltaV6,'x-c',Wavelength1,AvgDeltaV8,'x-y',Wavelength1,AvgDeltaV9,'x-
r',Wavelength11,AvgDeltaV11,'x-g',Wavelength,AvgDeltaV12,'x-b',Wavelength,AvgDeltaV13,'x-
k',Wavelength,AvgDeltaV14,'x-r',Wavelength,AvgDeltaV15,'x-b','LineWidth',2,'MarkerSize',10)
    hold all
    title('Average Change in Surface Voltage for Each Wafer')
    xlabel('Wavelength')
    xlim([425 825])
    ylabel('Average Change in Surface Voltage(V)')
    legend('Wafer #6','Wafer #8','Wafer #9','Wafer #11','Wafer #12','Wafer #13','Wafer #14','Wafer
#15','Simulation','Offset Simulation')
    %plot error bars for change in Voltage
    figure(3)
    errorbar(Wavelength1,AvgDeltaV6,StanD6,'x-c','LineWidth',2,'MarkerSize',10)
    legend('Wafer #6','Wafer #8','Wafer #9','Wafer #11','Wafer #12','Wafer #13','Wafer #14','Wafer
#15','Simulation','Offset Simulation')
    hold all
    figure(3)
    errorbar(Wavelength1,AvgDeltaV8,StanD8,'x-y','LineWidth',2,'MarkerSize',10)
    legend('Wafer #6','Wafer #8','Wafer #9','Wafer #11','Wafer #12','Wafer #13','Wafer #14','Wafer
#15','Simulation','Offset Simulation')
```

```
    hold all
    figure(3)
    errorbar(Wavelength1,AvgDeltaV9,StanD9,'x-r','LineWidth',2,'MarkerSize',10)
    legend('Wafer #6','Wafer #8','Wafer #9','Wafer #11','Wafer #12','Wafer #13','Wafer #14','Wafer
#15','Simulation','Offset Simulation')
    hold all
    figure(3)
    errorbar(Wavelength11,AvgDeltaV11,StanD11,'x-g','LineWidth',2,'MarkerSize',10)
    legend('Wafer #6','Wafer #8','Wafer #9','Wafer #11','Wafer #12','Wafer #13','Wafer #14','Wafer
#15','Simulation','Offset Simulation')
    hold all
    figure(3)
    errorbar(Wavelength,AvgDeltaV12,StanD12,'x-b','LineWidth',2,'MarkerSize',10)
    legend('Wafer #6','Wafer #8','Wafer #9','Wafer #11','Wafer #12','Wafer #13','Wafer #14','Wafer
#15','Simulation','Offset Simulation')
    hold all
    figure(3)
    errorbar(Wavelength,AvgDeltaV13,StanD13,'x-k','LineWidth',2,'MarkerSize',10)
    legend('Wafer #6','Wafer #8','Wafer #9','Wafer #11','Wafer #12','Wafer #13','Wafer #14','Wafer
#15','Simulation','Offset Simulation')
    hold all
    figure(3)
    errorbar(Wavelength,AvgDeltaV14,StanD14,'x-r','LineWidth',2,'MarkerSize',10)
    legend('Wafer #6','Wafer #8','Wafer #9','Wafer #11','Wafer #12','Wafer #13','Wafer #14','Wafer
#15','Simulation','Offset Simulation')
    hold all
    figure(3)
    errorbar(Wavelength,AvgDeltaV15,StanD15,'x-b','LineWidth',2,'MarkerSize',10)
    legend('Wafer #6','Wafer #8','Wafer #9','Wafer #11','Wafer #12','Wafer #13','Wafer #14','Wafer
#15','Simulation','Offset Simulation')
    hold all
    title('Average Change in Surface Voltage for Each Wafer')
    xlabel('Wavelength')
    xlim([425 825])
    ylabel('Average Change in Surface Voltage(V)')
    %determine drift of signal
    figure(4)
    plot(Wavelength1,MinV6,'x-c',Wavelength1,MinV8,'x-y',Wavelength1,MinV9,'x-
r',Wavelength11,MinV11,'x-g',Wavelength,MinV12,'x-b',Wavelength,MinV13,'x-
k',Wavelength,MinV14,'x-r',Wavelength,MinV15,'x-b','LineWidth',2,'MarkerSize',10)
    legend('Min Wafer #6','Min Wafer #8','Min Wafer #9','Min Wafer #11','Min Wafer #12','Min Wafer
#13','Min Wafer #14','Min Wafer #15','Max Wafer #6','Max Wafer #8','Max Wafer #9','Max Wafer
#11','Max Wafer #12','Max Wafer #13','Max Wafer #14','Max Wafer #15')
    hold all
    figure(4)
    plot(Wavelength1,MaxV6,'x--c',Wavelength1,MaxV8,'x--y',Wavelength1,MaxV9,'x--
r',Wavelength11,MaxV11,'x--g',Wavelength,MaxV12,'x--b',Wavelength,MaxV13,'x--
k',Wavelength,MaxV14,'x--r',Wavelength,MaxV15,'x--b','LineWidth',2,'MarkerSize',10)
    legend('Min Wafer #6','Min Wafer #8','Min Wafer #9','Min Wafer #11','Min Wafer #12','Min Wafer
#13','Min Wafer #14','Min Wafer #15','Max Wafer #6','Max Wafer #8','Max Wafer #9','Max Wafer
#11','Max Wafer #12','Max Wafer #13','Max Wafer #14','Max Wafer #15')
    title('Minimum and Maximum Surface Voltage for Each Wafer to Determine Drift')
    xlabel('Wavelength')
    xlim([425 825])
    ylabel('Min/Max Surface Voltage(V)')
%%Simulation
```

```
P= [1.29 5.73 9.16 12.1 17.8 17.6 9.49 0.229 .0256 ]; %power in mW at 100% intensity
Lstr={'400nm','450nm','500nm','550nm','600nm','650nm','700nm','750nm','800nm'};
lamda=[400 450 500 550 600 650 700 750 800];  %wavelength of light(nm)
lamda=lamda/10^(9); %wavelength of light(m)
alpha=[1*10^5 4*10^4 1.5*10^4 6.5*10^3 4.5*10^3 2.5*10^3 2*10^3 1.0*10^3 8.5*10^2];  %Si light absorption coefficent,Figure 3.20 (dependent on wavelngth)(/cm)
   %Define all constants
   h=4.136*10^(-15); %Planck's constant (eV*s)
   c=2.99*10^8; %speed of light in a vacuum (m/s)
   k=8.617*10^(-5); %Boltzman constant (eV/K)
   T=300;  %Temperature (K)
   q=1.602*10^(-19);  %unit of photon charge (C)
   einstein=0.0259;  %'Einstein constant', kT/q, at 300K (V)
   Epsilon0=8.8542*10^(-12)/100;  %permittivity of free space (C^2/J*cm)
   ni=1*10^(10); %intrinsic carrier concentration for Si at 300K (Fig 2.20)(/cm^3)
   Ks=11.8;  %Si dielectric Constant
   Ko=3.9;  %oxide dielectric Constant
   Ka=1; %air dielectric Constant
   Na=7*10^14;  %doping, Figure 3.8 (/cm^3) (considered not heavily doped!)
   EpsilonS=Ks*Epsilon0;  %permittivity of Si (C^2/J*cm)
   EpsilonOx=Ko*Epsilon0;  %permittivity of oxide (C^2/J*cm)
   chi=4.03; %intrinsic electron affinity work function (eV)
   EiEf=k*T*log(Na/ni); %difference between intrinsic Fermi level and doped Fermi level of Si  (eV)
   PhiSi=chi+EiEf+(1.01/2); %silicon work function (eV)
   PhiNi=5.01;  %Nickel work function (eV)
   Vcpd=((PhiNi-PhiSi)/q)*q; %contact potential difference between bulk Si and probe tip (V)
   B=2*10^(-15);  %material constant in Si (cm^3/s)
   %Define Si Wafer Properties
   rho=20;  %resistivity (Ohm/cm)
   Mup=459;  %Majority Carrier Mobility, Figure 3.5 (cm^2/(V-sec))
   Mun=1350;  %Minority Carrier Mobility, Figure 3.5 (cm^2/(V-sec))
   po=Na;  %majority carriers (/cm^3)
   no=(ni)^2/Na;  %minority carriers (/cm^3)
   Tauln=1.6*10^(-7);  %carrier lifetime (sec)  (Verify experimentally)
   Dn=einstein*Mun;  %diffusion constant related to Mu through Einstein Rel (cm^2/(sec))
   sFr=18000;  %front surface recombination velocity (cm/s)
   sBk=sFr;    %back surface recombination velocity (cm/s)
   Ln=sqrt(Dn*Tauln);%Minority Carrier Diffusion Lengths (cm);
   r=1;  %length of side  of aperture (cm)
   A=pi*r^2; %planar area of aperture (cm^2)
   dox=(47+74+79)/3*(1*10^(-8));  %average oxide thickness (cm)
   dair=1/10;  %average fly height(cm)
   C=((Epsilon0)*Ko*Ka)/(((dox)*Ka)+((dair)*Ko)); %capacitance of air and oxide layer (F/cm=C^2/Jcm)
   Q=C*Vcpd; %charge on the capacitor in the dark (C/cm)
for i=1:length(P)
   I=(P(i)/(1*10^3))/A;  %Intensity of light (W/cm^2)
   R=.32;
   Eph=h*c/(lamda(i)); %energy of a photon (eV)
   Nph=(I/(Eph*q)); %photon density per sec (photons/(cm^2*sec))
   alpha1=alpha(i);
   %Numerically find the number of excess electrons created by light
   %Call function to solve minority carrier diffusion Equation (BVP)
   NumDeltaN=MinorityCarriersSchroder(Ln,Dn,Nph,alpha1,R,sFr,sBk); %distribution of the # of excess electrons created (electron/um^2)
   NumDeltaN=NumDeltaN*(1*10^4)^2;  %distribution of the # of excess electrons created (electron/cm^2)
```

```
    NumDeltaNFr(i)=NumDeltaN(1); %# of excess electrons created at the surface (electron/cm^2)
    %%%Voltage Analysis%%%
    Qel=-NumDeltaNFr(i)*q; %amount of charge on the surface due to excess electrons (C/cm^2)
    Qex=Q+Qel;  %total amount of charge on the surface when light is present(C/cm^2)
    Vun=Vcpd; %surface voltage unexcited
    Vex=Qex/C; %surface voltage unexcited
    DeltaVSurface(i)=Vun-Vex;
end
Offset=0.02098985729882;
DeltaVSurface2=DeltaVSurface+Offset;
lamda=lamda*(1*10^9); %wavelength of light(nm)
figure(2)
plot(lamda,DeltaVSurface,'k-.','LineWidth',2,'MarkerSize',10)
hold all
legend('Wafer #6','Wafer #8','Wafer #9','Wafer #11','Wafer #12','Wafer #13','Wafer #14','Wafer
#15','Simulation','Offset Simulation')
figure(3)
plot(lamda,DeltaVSurface,'k-.','LineWidth',2,'MarkerSize',10)
hold all
legend('Wafer #6','Wafer #8','Wafer #9','Wafer #11','Wafer #12','Wafer #13','Wafer #14','Wafer
#15','Simulation','Offset Simulation')
figure(2)
plot(lamda,DeltaVSurface2,'r-.','LineWidth',2,'MarkerSize',10)
hold all
legend('Wafer #6','Wafer #8','Wafer #9','Wafer #11','Wafer #12','Wafer #13','Wafer #14','Wafer
#15','Simulation','Offset Simulation')
figure(3)
plot(lamda,DeltaVSurface2,'r-.','LineWidth',2,'MarkerSize',10)
hold all
legend('Wafer #6','Wafer #8','Wafer #9','Wafer #11','Wafer #12','Wafer #13','Wafer #14','Wafer
#15','Simulation','Offset Simulation')
```

Sub-functions

```
%Solve the BVP to final the distribution of excess electrons caused by
%light => assume steady state
function NumDeltaN=MinorityCarriersSchroder(Ln,Dn,Nph,alpha1,R,sFr,sBk);
options = [];
%change all length units to um
Ln=Ln*(1*10^4); %Minority Carrier Diffusion Lengths (um);
Dn=Dn*(1*10^4)^2;%diffusion constant related to Mu through Einstein Rel (um^2/(sec))
Nph=Nph/(1*10^4)^2;  %photon density per sec (photons/(um^2*sec))
alpha1=alpha1/(1*10^4);   %Si light absorption coefficent,Figure 3.20 (dependent on wavelngth)(/um)
sFr=sFr*(1*10^4);  %front surface recombination velocity (um/s)
sBk=sBk*(1*10^4);  %back surface recombination velocity (um/s)
solinit=bvpinit(linspace(0,650,500),[1 1]);  %create an initial guess of DeltaN=1 and DeltaN'=1 for one 500
points between x=-1000um and x=650um
sol=bvp4c(@Cont,@BCs,solinit,options,Ln,Dn,Nph,alpha1,R,sFr,sBk);  %evaluate the boundary value
problem
x=linspace(0,650,500);
y=deval(sol,x);
NumDeltaN=y(1,:); %# of excess Electrons created at steady state(electrons/(um^3))
%%-------------------------------------------------------------
function dydx=Cont(x,y,Ln,Dn,Nph,alpha1,R,sFr,sBk)
  dydx=[(y(2))
```

```
     (y(1)/(Ln^2)-(1-R)*Nph*alpha1*exp(alpha1*(x-650)))]
%%---------------------------------------------------------------
function res=BCs(ya,yb,Ln,Dn,Nph,alpha1,R,sFr,sBk)
   res=[(ya(2)-sFr*ya(1)/Dn)
      (yb(2)+sBk*yb(1)/Dn)];


%a function that designates a time scale for each set of data so that all of the curves can
%be plotted together for comparison
function t=zerostart(time)
deltatime=time(2)-time(1);
t(1)=0;
for n=2:length(time)
   t(n)=t(n-1)+deltatime;
end
```

APPENDIX B

LABVIEW PROGRAM

User Interface

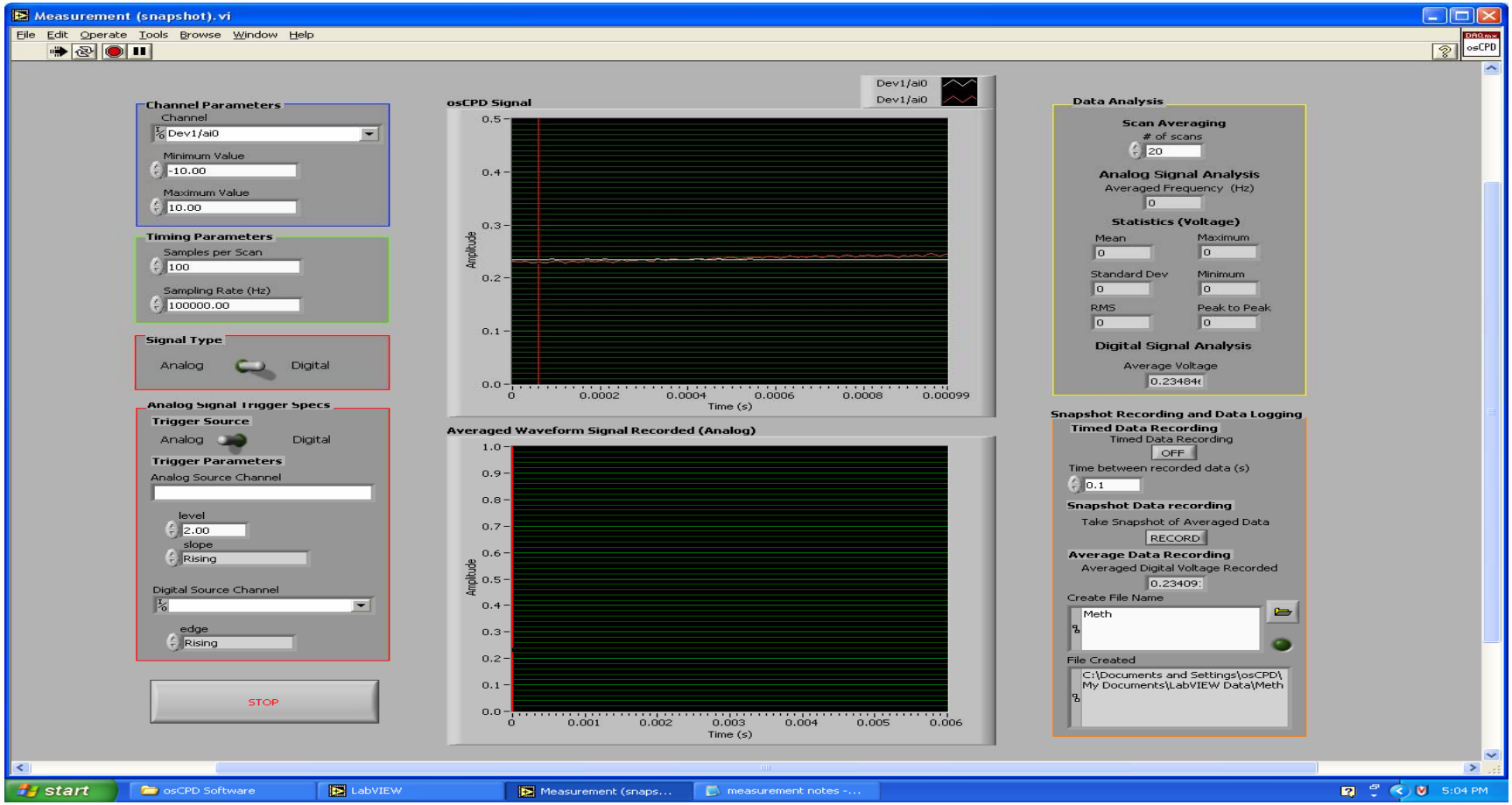

Block Diagram

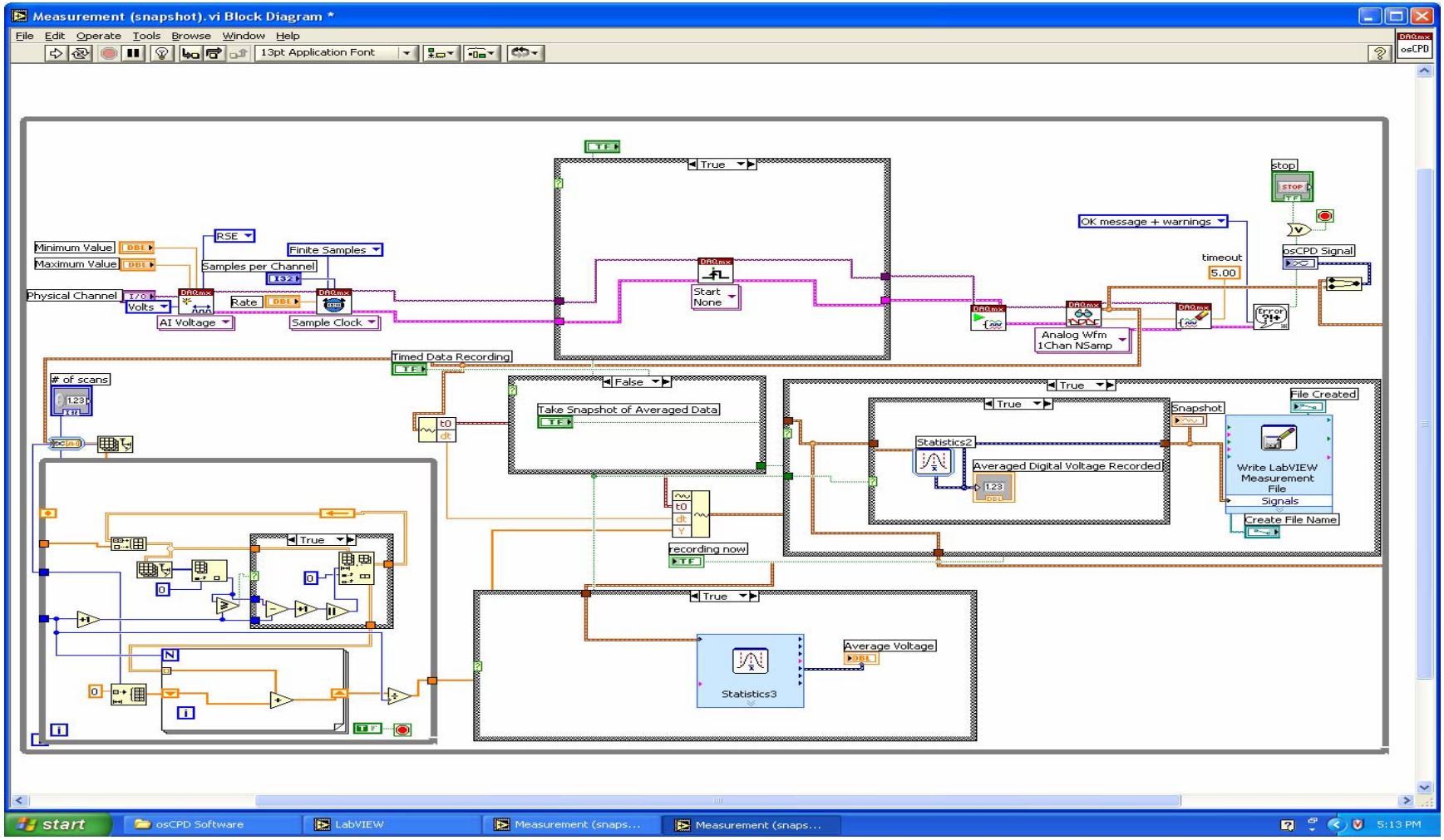

APPENDIX C

PARAMETER VALUES USED IN SIMULATION

$h = 4.136 \times 10^{-15}$ eVs	Planck's constant
$c = 2.99 \times 10^{8}$ m/s	Speed of light in a vacuum
$k = 8.617 \times 10^{-5}$ eV/K	Boltzman constant
T = 300 K	Temperature
$e = 1.602 \times 10^{-19}$ C	Unit of photon charge
$\varepsilon_0 = 8.8542 \times 10^{-12}$ C^2/Jm	Permittivity of free space
$Ni = 1 \times 10^{10}$ /cm^3	Intrinsic carrier concentration for Si at 300K
$K_s = 11.8$	Si dielectric Constant
$K_o = 3.9$	Oxide dielectric Constant
$K_a = 1$	Air dielectric Constant
Na = 7 x 10^^{14} /cm^3	Doping, Figure 3.8 [40]
$\chi = 4.03$ eV	Intrinsic electron affinity work function
$\varphi_{Ni} = 5.01$ eV	Nickel work function
$B = 2 \times 10^{-15}$ cm^3/s	Material constant in Si
$\rho = 20$ Ohm/cm	Resistivity
$\mu_p = 459$ cm^2/(V-sec)	Majority Carrier Mobility, Figure 3.5 [40]
$\mu_n = 1350$ cm^2/(V-sec)	Minority Carrier Mobility, Figure 3.5 [40]
$\tau_n = 1.6 \times 10^{-7}$ sec	Carrier lifetime for electrons
$s_{FRONT} = s_{REAR} = 18000$ cm/s	Front/rear surface recombination velocity

r = 1 cm	Radius of aperture hole
dair = 1/10 cm	Average fly height
R = 0.32	Reflectance of light

REFERENCES

1. Heerens, W.C., *Application of Capacitance Techniques in Sensor Design.* Journal of Physics E-Scientific Instruments, 1986. **19**(11): p. 897-906.

2. Kelvin, L.F., *Contact Electricity of Metals.* Philosophical Magazine Journal of Science, 1898. **46**(278): p. 82-120.

3. Zisman, W.A., *A new method of measuring contact potential differences in metals.* Review of Scientific Instruments, 1932. **3**(7): p. 367-370.

4. Craig, P.P. and V. Radeka, *Stress Dependence of the Contact Potential: The ac Kelvin Method.* Review of Scientific Instruments, 1969. **41**(2): p. 258-264.

5. Stratmann, M. and H. Streckel, *The Investigation of the Corrosion of Metal Surfaces Covered with Thin Electrolyte Layers - A New Experimental Technique.* Berichte Der Bunsen-Gesellschaft-Physical Chemistry Chemical Physics, 1988. **92**(11): p. 1244-1250.

6. Beltzer, M., *Assessing Adsorption of Conventional Friction Modifying Molecules by Relative Contact Potential Difference Measurements.* Journal of Tribology-Transactions of the ASME, 1992. **114**(4): p. 675-682.

7. Butz, R. and H. Wagner, *A Device for Measuring Contact Potential Differences with High Spatial Resolution.* Applied Physics, 1977. **13**(1): p. 37-42.

8. Kasai, T., et al., *Applications of a Non-contacting Kelvin probe During Sliding* Wear, 1999. **229**: p. 1186-1204.

9. Zharin, A. and D. Rigney, *Application of the Contact Potential Difference Technique for On-line Rubbing Surface Monitoring (Review).* Tribology Letters, 1998. **4**: p. 205-213.

10. Danyluk, S., *UHV Guarded Kelvin Probe* Journal of Physics E-Scientific Instruments, 1972. **5**(5): p. 478-480.

11. Sze, S.M., *Physics of Semiconductor Devices*. Second ed. 1981, New York: John Wiley & Sons.

12. Pierret, R.F., *Semiconductor Device Fundamentals*. 1996, New York Addison Wesley Longman.

13. Garrett, C.G.B. and W.H. Brattain, *Physical Theory of Semiconductor Surfaces.* Physical Review 1955. **99**(2): p. 376-387.

14. Karazhanov, S.Z., *Impurity photovoltaic effect in indium-doped silicon solar cells.* Journal of Applied Physics, 2001. **89**(7): p. 4030-4036.

15. Cavalcoli, D., et al., *Surface contaminant detection in semiconductors using non-contacting techniques.* Journal of the Electrochemical Society, 2003. **150**(8): p. G456-G460.

16. Lagel, B., M.D. Ayala, and R. Schlaf, *Kelvin probe force microscopy on corona charged oxidized semiconductor surfaces.* Applied Physics Letters, 2004. **85**(20): p. 4801-4803.

17. Kamins, T.I. and B.E. Deal, *Characteristics of Si-SiO2 Interfaces beneath Thin Silicon Films Defined by Electromechanical Etching.* Journal of the Electrochemical Society, 1975. **122**(4): p. 557-560.

18. Massies, J., P. Devoldere, and N.T. Linh, *Work Function Measurements on MBe GaAs(001) Layers.* Journal of Vacuum Science & Technology, 1979. **16**(5): p. 1244-1247.

19. Leer, J.v. and A. Huijser, *Contact Potential Differences for III-V Compound Surfaces.* Journal of Vacuum Science Technology, 1976. **13**(4): p. 769-772.

20. Glatzel, T., et al., *Kelvin probe force microscopy on III-V semiconductors: the effect of surface defects on the local work function.* Materials Science and Engineering B-Solid State Materials for Advanced Technology, 2003. **102**(1-3): p. 138-142.

21. Tsurekawa, S., K. Kido, and T. Watanabe, *Measurements of potential barrier height of grain boundaries in polycrystalline silicon by Kelvin probe force microscopy.* Philosophical Magazine Letters, 2005. **85**(1): p. 41-49.

22. Johnson, E.O., *Measurement of Minority Carrier Lifetimes with the Surface Voltage.* Journal of Applied Physics, 1957. **28**(11): p. 1349-1353.

23. Schoder, D.K., *Surface Voltage and Surface Photovoltage: History, Theory, and Applications.* Measurement Science and Technology, 2001. **12**: p. R16-R31.

24. Mess, F., *A Novel Sensor to Monitor Surface Charge Interactions: The Optically Stimulated Contact Potential Difference Probe*, in *PhD Thesis*. 2006, Georgia Institute of Technology: Atlanta.

25. Zharin, A.L. and G.P. Shpenkov, *Macroscopic Effects of Delamination Wear.* Wear, 1979. **56**(2): p. 309-313.

26. Shampine, L.F., M.W. Reichelt, and J. Kierzenka, *Solving Boundary Value Problems for Ordinary Differential Equations in MATLAB with bvp4c.*

27. Brody, J., A. Rohatgi, and A. Ristow, *Review and comparison of equations relating bulk lifetime and surface recombination velocity to effective lifetime measured under flash lamp illumination.* Solar Energy Materials and Solar Cells, 2003. **77**(3): p. 293-301.

28. Zanoria, E.S., et al., *Contact potential measurements of hard disk drive surfaces in humid environments.* Journal of Vacuum Science & Technology a-Vacuum Surfaces and Films, 1996. **14**(1): p. 52-55.

29. Kronik, L. and Y. Shapira, *Surface Photovoltage Spectroscopy of Semiconductor Structures: at the Crossroads of Physics, Chemistry, and Electrical Engineering.* Surface and Interface Analysis, 2001. **31**: p. 954-965.

30. Kropman, D., et al., *Interaction between point defects, extended defects and impurities in the Si-SiO2 system during the process of its formation.* Materials

Science and Engineering B-Solid State Materials for Advanced Technology, 2004. **114-15**: p. 295-298.

31. Ishii, M. and B. Hamilton, *Time transient investigation of photo-induced electron localization at atomic step edges of Si(111).* Applied Surface Science, 2005. **248**(1-4): p. 14-18.

32. Leibovitch, M., et al., *Constructing Band Diagrams of Semiconductor Heterojunctions.* Applied Physics Letters, 1995. **66**(4): p. 457-459.

33. Deal, B.E., et al., *Characteristics of the Surface-State Charge (Qss) of Thermally Oxidized Silicon.* Journal of the Electrochemical Society, 1967. **114**(3): p. 266-274.

34. Kobayashi, H., et al., *Mechanism of Open-Circuit Photovoltages for Silicon-Methanol Junction Solar Cells.* Journal of Electroanalytical Chemistry, 1995. **398**(1-2): p. 165-168.

35. Xie, Z.X., et al., *Dissociation mechanism of methanol on a Si(111)-(7x7) surface studied by scanning tunneling microscopy.* Physical Review B, 2002. **66**(12).

36. Michalak, D.J., et al., *Infrared spectroscopic investigation of the reaction of hydrogen-terminated, (111)-oriented, silicon surfaces with liquid methanol.* Journal of Physical Chemistry B, 2006. **110**(41): p. 20426-20434.